

University of Groningen

## Adaptive fault-tolerant attitude tracking control for hypersonic vehicle with unknown inertial matrix and states constraints

Wang, Le; Meng, Yizhen; Hu, Shiqi; Peng, Zhiyu; Shi, Wen

*Published in:*  
IET Control Theory and Applications

*DOI:*  
[10.1049/cth2.12470](https://doi.org/10.1049/cth2.12470)

**IMPORTANT NOTE:** You are advised to consult the publisher's version (publisher's PDF) if you wish to cite from it. Please check the document version below.

*Document Version*  
Publisher's PDF, also known as Version of record

*Publication date:*  
2023

[Link to publication in University of Groningen/UMCG research database](#)

### *Citation for published version (APA):*

Wang, L., Meng, Y., Hu, S., Peng, Z., & Shi, W. (2023). Adaptive fault-tolerant attitude tracking control for hypersonic vehicle with unknown inertial matrix and states constraints. *IET Control Theory and Applications*, 17(10), 1397-1412. <https://doi.org/10.1049/cth2.12470>

### **Copyright**

Other than for strictly personal use, it is not permitted to download or to forward/distribute the text or part of it without the consent of the author(s) and/or copyright holder(s), unless the work is under an open content license (like Creative Commons).

The publication may also be distributed here under the terms of Article 25fa of the Dutch Copyright Act, indicated by the "Taverne" license. More information can be found on the University of Groningen website: <https://www.rug.nl/library/open-access/self-archiving-pure/taverne-amendment>.

### **Take-down policy**

If you believe that this document breaches copyright please contact us providing details, and we will remove access to the work immediately and investigate your claim.

Downloaded from the University of Groningen/UMCG research database (Pure): <http://www.rug.nl/research/portal>. For technical reasons the number of authors shown on this cover page is limited to 10 maximum.

## ORIGINAL RESEARCH

# Adaptive fault-tolerant attitude tracking control for hypersonic vehicle with unknown inertial matrix and states constraints

Le Wang<sup>1</sup>  | Yizhen Meng<sup>2</sup> | Shiqi Hu<sup>3</sup>  | Zhiyu Peng<sup>4,5</sup> | Wen Shi<sup>4,5</sup>

<sup>1</sup>College of Automation Engineering, Nanjing University of Aeronautics and Astronautics, Nanjing, China

<sup>2</sup>Shanghai Key Laboratory of Aerospace Intelligent Control Technology, Shanghai Aerospace Control Technology Institute, Shanghai, China

<sup>3</sup>College of Food Science and Technology, Nanjing Agricultural University, Nanjing, China

<sup>4</sup>School of Automation, Southeast University, Nanjing, China

<sup>5</sup>Engineering and Technology Institute Groningen, Faculty of Science and Engineering, University of Groningen, Groningen, The Netherlands

## Correspondence

Shiqi Hu, College of Food Science and Technology, Nanjing Agricultural University, Nanjing, 210095, China.  
Email: hushiqi@njau.edu.cn

## Present address

Shiqi Hu, College of Food Science and Technology, Nanjing Agricultural University, Nanjing 210095, China

## Funding information

Postgraduate Research and Practice Innovation Program of Jiangsu Province, Grant/Award Numbers: KYCX20\_0207, KYCX20\_0572; Interdisciplinary Innovation Foundation for Graduates, NUAA, Grant/Award Number: KXXCXJJ202008; China Scholarship Council, Grant/Award Numbers: 202206090189, 202206090190

## Abstract

This paper proposes an adaptive fault-tolerant control (FTC) method for hypersonic vehicle (HSV) with unexpected centroid shift, actuator fault, time-varying full state constraints, and input saturation. The occurrence of unexpected centroid shift has three main effects on the HSV system, which are system uncertainties, eccentric moments, and variation of input matrix. In order to ensure the time-varying state constraints, a novel attitude state constraint control strategy, to keep the safe flight of HSV, is technically proposed by a time-varying state constraint function (TVSCF). A unified controller is designed to handle the time-varying state constraints according to the proposed TVSCF. Then, the constrained HSV system can be transformed into a novel free-constrained system based on the TVSCF. For the variation of system input matrix, input saturation and actuator fault, a special Nussbaum-type function is designed to compensate for those time-varying nonlinear terms. Additionally, the auxiliary systems is designed to compensate the constraint of system control inputs. Then, it is proved that the proposed control scheme can guarantee the boundedness of all closed-loop signals based on the Lyapunov stability theory. At last, the simulation results are provided to demonstrate the effectiveness of the proposed fault-tolerant control scheme.

## 1 | INTRODUCTION

Atmospheric reentry technology is regarded as the basis for a wide range of space applications, such as planetary exploration, specimen return, the development of future vehicles and space planes, space transportation of crew and cargo, unmanned aerial vehicles serving satellites in orbit and other innovative applications in aerospace field. During the past decades, reentry guidance and control problems have become the research

hotspots in the aerospace field [1, 2]. So far, hypersonic vehicle (HSV) has been the most complicated flight process because it provides a more reliable and cost efficient way to access space. Especially for the reentry stage of HSV, it is necessary to guide the HSV to a given landing area smoothly and safely under the condition of great initial reentry kinetic energy and potential energy [3]. At the same time, the overload, dynamic pressure and aerodynamic heating are kept within the allowable range, which is the main challenge for the guidance and control design of the

This is an open access article under the terms of the [Creative Commons Attribution-NonCommercial-NoDerivs](https://creativecommons.org/licenses/by-nc-nd/4.0/) License, which permits use and distribution in any medium, provided the original work is properly cited, the use is non-commercial and no modifications or adaptations are made.

© 2023 The Authors. *IET Control Theory & Applications* published by John Wiley & Sons Ltd on behalf of The Institution of Engineering and Technology.

re-entry stage of the HSV, and it is also the distinguishing feature of other aircraft [4]. The reentry phase of HSV has the following characteristics: large airspace, transonic speed, multi-stage, nonlinear, strong coupling, severe constraints and severe uncertainty [5, 6]. In recent years, there have been a great number of research results, such as predictive control [7], fuzzy control [8], optimal control [9], adaptive sliding mode control [10] and robust control [11].

The task of HSV attitude control in the reentry phase is to make the vehicle track the angle of attack and pitch angle commands provided by the guidance loop, while ensuring the sideslip angle to be near zero. The papers [12, 13] develop Euler equation to describe the dynamic model of X233 reentry into the atmosphere, and design two sliding mode controllers. The sliding mode controller of the inner loop is designed for the dynamic model of the aircraft, and the sliding mode controller of the outer loop is designed for the kinematic model of the angular velocity of the aircraft. The biggest advantage of this control scheme is that it can achieve the tracking of a given angle and angular velocity command at the same time. The paper [14] designs a feedback linearized controller based on the concept of time scale separation for lift-type reentry vehicles to track the guidance commands of standard orbits. Combined feedback linearization with proportional-integral-derivative, the paper [15] designs a tracking controller for the reentry vehicle to track the desired angle of attack and  $X$ -axis angular rate. The paper [16] studies the attitude control problem of X-38 re-entry into the atmosphere based on the method of fuzzy logic. The whole process of the re-entry vehicle is divided into five stages, and each flight stage corresponds to different actuator structures. In [17], for the uncertainty of the flight dynamics characteristics of HSV, the re-entry attitude control problem is demonstrated to obtain robustness against uncertainty based on  $H^\infty$  control theory and model-following adaptive control theory. However, when HSV control surface faults and structural damages occur during the reentry process, the above methods often fail to meet the stringent requirements for autonomy and safety. Therefore, it is necessary to consider the possible faults of the system when designing the attitude controller, and fault-tolerant control is crucial for HSV to guarantee its safety and achieve the control goal.

For the variation of aircraft centroid, it is an serious and complex fault-tolerant control (FTC) problem of HSV [18]. The occurrence of unexpected centroid shift has three main effects on the HSV system, which are system uncertainties, eccentric moments, and variation of input matrix [19]. The nonlinear aircraft dynamics with unexpected centroid shift are presented in [19]. In [20], a novel adaptive control scheme is introduced to handle the centroid shift fault. In [21], a linearized HSV model with unexpected centroid shift problem is described. However, the linearized model may trigger the absence of the system coupling, resulting in the performance degradation of the controller, especially what a fault occurrence. For the variation of the inertial matrix, the paper [22] tries to resolve such a problem by assuming that the minimum and maximum bounds of the inertial matrix are known, but this assumption restricts the application of this strategy because the mentioned bounds are

hard to be obtained. Besides, based on data-driven techniques [23], a model free control scheme is proposed for the uncertainties of system. However, it should be noted that it is difficult to obtain the training data of the inertial matrix of HSV with centroid shift. In a word, how to online identify the inertial matrix of the HSV with uncertainties and ensure its function in a FTC controller is still full of challenges.

In summary, it is an interesting and important topic to investigate the FTC problem of HSV subject to an unexpected centroid shift, actuator fault, time-varying full state constraints and system input saturation. The major contributions are summarized as follows:

- (i) Compared with the former FTC methods, the time-varying full state constraints are first applied into the FTC algorithm designed in this paper for the HSV with unknown inertial matrix, eccentric moment, external disturbance, actuator fault and system input saturation, and the desired tracking performance can be achieved.
- (ii) A special auxiliary system based on a Nussbaum-type function is designed to eliminate the effects of the unknown inertial matrix, actuator fault and input constraints, which can be regarded as a complement to the FTC algorithm.
- (iii) To handle the problem of the time-varying state constraints, a time-varying state constraint function (TVSCF) is developed so that the constrained HSV system can be transformed into a novel free-constrained system.

The article is organized in the following parts. Section 2 is devoted to establish the model of HSV with unexpected centroid shift, actuator fault, and so forth. Section 3 gives some definitions and preliminaries. Subsequently, the adaptive fault-tolerant anti-saturation controller is proposed in Section 4. The stability analysis is proposed in Section 5 and followed by Section 6, in which the numerical simulations are conducted to evaluate the effectiveness of the designed FTC algorithm. Finally, the conclusion is provided in Section 7.

## 2 | PROBLEM FORMULATION

### 2.1 | HSV attitude dynamics with unexpected centroid shift

#### 2.1.1 | Attitude angle dynamic equation

The reentry attitude dynamics of hypersonic vehicle considered in this paper are given by [24]. The attitude system of HSV is described by

$$\dot{\gamma} = \mathfrak{R}(\gamma)\omega, \quad (1)$$

where  $\gamma = [\mu, \alpha, \beta]^T$  denotes the attitude angle vector, and  $\omega = [p, q, r]^T$  represents the angular rate vector.  $\mu, \alpha, \beta, p, q$  and  $r$  represent the bank angle, the angle of attack, the sideslip angle, roll rate, pitch rate and yaw rate, respectively. The rotational

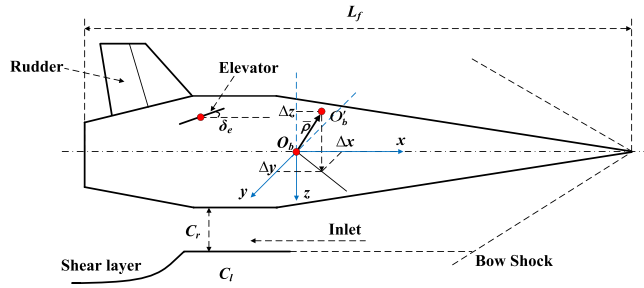


**FIGURE 1** Three-dimensional view of HSV with centroid shift,  $O_b \rightarrow O'_b$ .

matrix  $\mathfrak{R}(\gamma)$  in (1) is expressed as

$$\mathfrak{R}(\gamma) = \begin{bmatrix} \cos \alpha & 0 & \sin \alpha \\ \sin \alpha & 0 & -\cos \alpha \\ 0 & 1 & 0 \end{bmatrix}, \quad (2)$$

### 2.1.2 | Attitude angular rate dynamic equation

As depicted in Figure 1, the centroid shift refers to the phenomenon that the original centroid of the HSV ( $O_b$ ) moves to the new location ( $O'_b$ ). Inspired by the work in [25] and [26], the HSV attitude angular rate dynamic with unexpected centroid shift, system uncertainty and external disturbance can be developed as

$$(J^* + \Delta J)\dot{\omega} = -\omega^\times (J^* + \Delta J)\omega + \Lambda + v + d, \quad (3)$$

where  $J^* \in R^{3 \times 3}$  represents the inertial matrix of the HSV without uncertainties, and it is displayed as follows:

$$J^* = \begin{bmatrix} J_{xx} & 0 & -J'_{xz} \\ 0 & J_{yy} & 0 \\ -J'_{xz} & 0 & J_{zz} \end{bmatrix}, \quad (4)$$

where  $J_{xx}, J_{yy}, J_{zz}$  denote the moments of inertia.  $J'_{xz}$  is the product of inertia.  $d$  stands for the external disturbance moment. Besides, the operator  $\omega^\times$ , which is a skew-symmetric matrix acting on  $\omega$ , can be expressed as follows:

$$\omega^\times = \begin{bmatrix} 0 & -r & q \\ r & 0 & -p \\ -q & p & 0 \end{bmatrix}. \quad (5)$$

In what follows, based on previous research in [26–28], it can be concluded that the effects of centroid shift are mainly in these three aspects: (a) variation of inertial matrix; (b) system uncertainty; and (c) eccentric moment, and the details are delivered as follows:

- (a) *Variation of inertial matrix:*  $\Delta J \in R^{3 \times 3}$  represents an uncertain part of  $J^*$  which results from the centroid shift, and it is delivered as

$$\Delta J = \begin{bmatrix} \Delta J_{xx} & -J_{xy} & -J_{xz} \\ -J_{xy} & \Delta J_{yy} & -J_{yz} \\ -J_{xz} & -J_{yz} & \Delta J_{zz} \end{bmatrix} \quad (6)$$

where  $J_{xy}, J_{xz}$  and  $J_{yz}$  are the products of inertia which results from the unknown centroid shift vector  $\bar{p} = [\Delta x, \Delta y, \Delta z]^T$ , presented in Figure 1. The expressions of the uncertain inertial matrix are [29]:

$$\Delta J_{xx} = M(\Delta y^2 + \Delta z^2), \quad (7a)$$

$$\Delta J_{yy} = M(\Delta x^2 + \Delta z^2), \quad (7b)$$

$$\Delta J_{zz} = M(\Delta x^2 + \Delta y^2), \quad (7c)$$

$$\Delta J_{xy} = M\Delta x\Delta y, \quad (7d)$$

$$\Delta J_{xz} = M\Delta x\Delta z, \quad (7e)$$

$$\Delta J_{yz} = M\Delta y\Delta z. \quad (7f)$$

where  $M$  represents the mass of HSV.  $\Delta x, \Delta y$  and  $\Delta z$  are the three components of the centroid shift vector  $\bar{p}$  along the aircraft body frame  $O_{bxyz}$ . It is worth noting that due to the existence of the uncertain inertial matrix ( $J^* + \Delta J$ ), it is difficult to construct the controller by inverting inertial matrix, such as backstepping control [30], dynamics surface control [31], and so on.

- (b) *System uncertainty:* In this paper, by multiplying the inverse matrix  $(J^* + \Delta J)^{-1}$  to the both sides of (3), it can be seen that the system uncertainty caused by  $\Delta J$  is difficult to separate from  $-(J^* + \Delta J)^{-1}\omega^\times (J^* + \Delta J)\omega$ . Furthermore, based on (3), (6) and (7), one has  $J_{xy} \neq 0$  and  $J_{yz} \neq 0$  when  $[\Delta x, \Delta y, \Delta z]^T \neq 0$ . Therefore,  $(J^* + \Delta J)$  has become a coupled matrix instead of  $J^*$ .
- (c) *Eccentric moment:* The unexpected centroid shift results in the occurrence of eccentric moment  $\Lambda$  which is formulated by

$$\Lambda = \begin{bmatrix} 0 & -v_z & v_y \\ v_z & 0 & -v_x \\ -v_y & v_x & 0 \end{bmatrix} \begin{bmatrix} \Delta x \\ \Delta y \\ \Delta z \end{bmatrix} = \Theta^\times \zeta \quad (8)$$

where  $v_x, v_y$  and  $v_z$  represent the three components of the moment vector  $v$  along the aircraft body coordinate  $O_{bxyz}$ , which is depicted in Figure 1.

## 2.2 | Actuator fault and system input saturation

As for control moment vector  $v$  in (3),  $v = [v_1, v_2, v_3]^T$  is the function of  $\delta$ , and it is described as

$$v = BFu(\delta) + B\bar{u}, \quad (9)$$

where  $B \in R^{3 \times 8}$  is the actuator distribution matrix that characterizes the effect of each control surface on the angular rate system.  $u(\delta)$  stands for the control input with saturation nonlinearities. In this paper, X-33 has four sets of control surfaces, such as rudders, body flaps, and inboard and outboard elevons, respectively. It can be represented by  $\delta = [\delta_1, \delta_2, \dots, \delta_8]^T$ .  $F = \text{diag}\{f_{i1}, f_{i2}, \dots, f_{i8}\}$  with  $0 \leq f_{ii} \leq 1$  ( $i = 1, 2, \dots, 8$ ) represents the fault matrix that reflects the health condition of the corresponding actuator, and  $\bar{u}$  denotes the unexpected control moment caused by actuator fault and other reasons. With this setting, the following common fault types of actuator can be taken into consideration: a) partial loss of effectiveness; b) locking; and c) null and continuous bias [32].

Considering actuator symmetric input constraints,  $u(\delta_i)$  represents the controller with input saturation, shown as [33]

$$u(\delta_i) = \text{sat}(\delta_i) = \begin{cases} \delta_{i\max}, & \delta_i > \delta_{i\max} \\ \delta_i, & |\delta_i| \leq \delta_{i\max} \\ \delta_{i\min}, & \delta_i < -\delta_{i\max} \end{cases} \quad (10)$$

where  $\delta_{i\max}$  is the maximum deflection angle of control surfaces  $\delta_i$ . Then, define  $\kappa(\delta) = [\kappa_1(\delta_1), \kappa_2(\delta_2), \dots, \kappa_8(\delta_8)]^T$ , and a hyperbolic tangent function is applied to approximate  $u(\delta)$  in (10):

$$u(\delta) = \kappa(\delta) + \varepsilon(\delta), \quad (11)$$

$$\kappa_i(\delta_i) = \delta_{i\max} \tanh(\delta_i / \delta_{i\max}), \quad (12)$$

where  $\varepsilon(\delta_i)$  represents the fitting error, which satisfies  $|\varepsilon_i(\delta_i)| = |\text{sat}(\delta_i) - \kappa_i(\delta_i)| \leq \delta_{i\max}(1 - \tanh(1))$ .

According to the mean-value theorem and the assumption that  $\kappa(0) = 0$  [34], it is obtained that

$$\kappa_i(\tau_i) = \frac{\partial \kappa_i(\cdot)}{\partial \delta_i} \delta_i = b_i \delta_i. \quad (13)$$

In addition, define  $H = \text{diag}\{b_i\}$ ,  $i = 1, 2, \dots, 8$ , and (11) can be reformed as  $u(\delta) = H\delta + \varepsilon(\delta)$ . Thus, the control moment vector in (9) can be rewritten as

$$v = BY\delta + B(F\varepsilon(\delta) + \bar{u}) \quad (14)$$

where  $Y = \text{diag}\{f_{ii}b_i\}$ ,  $i = 1, 2, \dots, 8$ . It should be mentioned that the matrix  $Y$  is time-varying which reflects the control surface fault and saturation.

## 2.3 | Problem statement

Considering the HSV attitude model with unexpected centroid shift, actuator fault and input saturation, an adaptive fault-tolerant control scheme is designed to fulfil the following control objectives:

- (i) The system output  $\gamma = [\alpha, \beta, \mu]^T$  tracks the desired trajectory  $\gamma_r = [\alpha_r, \beta_r, \mu_r]^T$ , and the steady-state behavioural boundedness of the attitude angles is preserved.
- (ii) All signals are bounded and stable in the entire closed-loop system.

Before designing the fault-tolerant controller, some assumptions are needed.

**Assumption 1.** The desired tracking command signals  $\gamma_r$  and its time-derivative  $\dot{\gamma}_r$  is continuous and bounded. Moreover, all states of the HSV attitude model are available.

**Assumption 2.** The inverse matrix  $J^{-1} = (J^* + \Delta J)^{-1}$  exists.

**Assumption 3.** The eccentric moment  $\Lambda$  is uncertain but bounded, which satisfies  $\|\Lambda\| \leq \kappa_\Lambda$  with  $\kappa_\Lambda$  being a positive constant. In addition, the disturbance  $d$  in (3) satisfies  $\|d\| \leq \ell_d$ , where  $\ell_d$  represents an unknown positive constant.

**Assumption 4.** In this paper, we focus on the fault-tolerant control strategy. Thus, the time of fault occurrence is assumed to be known in this paper and it is regarded as a sign that system state constraints are needed. The time of fault occurrence can be obtained by the methods shown in [35, 36].

*Remark 1.* Assumption 1 ensures the desired trajectory  $\gamma_r$  and its derivatives to be bounded, and it is frequently employed in current relevant literatures [26]. In addition, the states of the HSV system can be measured by various sensors on the aircraft, and this assumption is mainly for convenience of designing the state feedback controller [9]. According to the discussion in [27] and [28], it can be obtained that when the centroid of the HSV shifts, the variation of the moment of inertia  $J$  will not affect the invertibility of the matrix  $J^* + \Delta J$ , so Assumption 2 is reasonable. Assumption 3 indicates that the eccentric moment which results from the unexpected centroid shift is bounded, and such an assumption also appears in [26–29].

## 3 | PRELIMINARY KNOWLEDGE

### 3.1 | Time-varying state-constraint function

A continuous function  $\zeta(\cdot)$  is defined as a time-varying state constraint function if it is endorsed by the following property:

$$\zeta(t) = \frac{x(t)}{(F_1(t) + x(t))^T (F_2(t) - x(t))}, \quad (15)$$

where the initial condition  $x(0)$  satisfies  $x(0) \in \mathcal{G}$ , and both  $F_1(t)$  and  $F_2(t)$  are time-varying constraint functions. Through an inspection of (16), it is straightforward to verify that  $\zeta$  approaches infinity as  $x$  tends to the boundary of  $\mathcal{G} := [-F_1(t), F_2(t)]$ , that is, for any initial state  $x(0) \in \mathcal{G}$

$$\zeta \rightarrow \pm\infty \text{ if and only if } x \rightarrow -F_1(t) \text{ or } x \rightarrow F_2(t) \quad (16)$$

The prominent property of the designed TVSCF is that for any  $x(T) \in \mathcal{G}$ , if  $\zeta \in L_\infty$  for any  $t \geq T$ , it is sufficient to achieve that  $x(t) \in \mathcal{G}$ , that is to say, the state constraints can be guaranteed if only  $\zeta$  is ensured to be bounded. Therefore, the problem of state constraints can be attributed to making sure the boundedness of  $\zeta$  for all  $t \geq T$ .

**Remark 2.** Examining (15) with respect to  $F$ , an important aspect that deserves attention is that the case of setting  $F_j \rightarrow \infty$  combined with the rule of L.Hospital makes

$$\lim_{F_j \rightarrow \infty} \frac{x_j}{(F_j + x_j)(F_j - x_j)} = x_j \quad (17)$$

where  $F_j$ ,  $j = 1, 2, 3$  stands for the element of  $F$ , and it is an important property when it comes to the fault-tolerant control:

- (1) When a fault occurs, the extra states constraints should be made for the requirement of safety. To this aim, a safety aero  $\mathcal{G}$  described by  $F$  is proposed, as shown in (15) and (16);
- (2) As for the normal condition, namely, without resorting to the additional state constraints, combined with (17), it is apparent that (15) can be transformed as a common state of HSV.

Contrary to the common practice with respect to the barrier Lyapunov function (BLF) [37, 38], shown as

$$V_b = \frac{1}{2} \log \frac{\mathfrak{F}_b^2}{\mathfrak{F}_b^2 - \tilde{x}^T \tilde{x}} \quad (18)$$

where  $\tilde{x}$  represents the constrained variable and  $\mathfrak{F}_b$  is the constraint bound value, that is,  $V_b \rightarrow \infty$  if  $\|\tilde{x}\| \rightarrow \mathfrak{F}_b$ . However, if the constraint requirement is not required in normal condition, that is,  $V_b \rightarrow \infty$ , then  $V_b \rightarrow 0$  instead of the Lyapunov quadratic form  $\tilde{x}^T \tilde{x}/2$ , which means that the usual BLF can not handle the cases with or without constraints in a unified scheme. In this work, a novel BLF is presented to handle the system with or without the states constraint requirements in a unified way by adjusting the parameters of  $F(t)$ .

In addition, for the time-varying constraint functions, a mild assumption is provided as follows:

**Assumption 5.** The constraint function  $F_j(t)$  is positive and time-varying, and its  $k$ th derivative ( $k = 0, 1, 2$ ) is bounded and continuous.

**Remark 3.** There exist some positive constant vectors  $L_0, L_1$ , and  $L_2$ , so that the desired signal  $\gamma_{ri}(t)$ ,  $i = 1, 2, 3$  and its time derivatives  $\dot{\gamma}_{ri}, \ddot{\gamma}_{ri}$  satisfy  $\gamma_{ri} \in D_c := \{\gamma_{ri} \in R : -F_i(t) < -L_{0i} \leq \gamma_{ri}(t) \leq L_{0i} < F_i(t)\}$  and  $|\gamma_{ri}^{(l)}(t)| < L_{li}$ . What is more,  $[\gamma_{ri}, \dot{\gamma}_{ri}, \ddot{\gamma}_{ri}]^T \in \Omega_{\gamma_r}$  is continuous and available in the known compact set  $\Omega_{\gamma_r} := \{[\gamma_{ri}, \dot{\gamma}_{ri}, \ddot{\gamma}_{ri}]^T : \gamma_{ri} + \dot{\gamma}_{ri} + \ddot{\gamma}_{ri} \leq B_0\} \subset R^3$ , where  $B_0$  is a positive constant.

### 3.2 | Nussbaum-type function

A Nussbaum function is firstly proposed to be a control-direction selector [39]. Since the matrix  $Y$  in (14) is time-varying, we use the Nussbaum gain to estimate it in this paper.

**Definition 1.** The properties of Nussbaum-type function  $N(\cdot)$  are introduced as follows [34, 38]:

$$\begin{aligned} \lim_{\vartheta \rightarrow \infty} \inf \frac{1}{\vartheta} \int_0^{\vartheta} N(\xi) d\xi &= -\infty \\ \lim_{\vartheta \rightarrow \infty} \sup \frac{1}{\vartheta} \int_0^{\vartheta} N(\xi) d\xi &= +\infty \end{aligned} \quad (19)$$

Based on (19), the Nussbaum function is developed as

$$N(\xi) = e^{\xi^2/2} (\xi^2 + 2) \sin(\xi). \quad (20)$$

**Lemma 1** [34].  $V(t)$  and  $\xi_i(t)$  ( $i = 1, 2, \dots, m$ ) are assumed as the smooth functions in  $[0, t_f]$  with  $V(t) \geq 0$  and  $\xi_i(0) = 0$ . If  $N(\cdot)$  satisfied (20) and the following inequality holds

$$\dot{V}(t) = c_0 + e^{-c_1 t} \sum_{i=1}^N \int_0^t (-g_i(\tau) N(\xi_i(\tau)) + 1) \dot{\xi}_i(\tau) e^{c_1 \tau} d\tau \quad (21)$$

where  $c_0$  represents a bounded constant, then  $V(t)$ ,  $\xi_i(t)$  and  $\sum_{i=1}^N \int_0^t g_i(\tau) N(\xi_i(\tau)) \dot{\xi}_i(\tau) d\tau$  are bounded on  $[0, t_f]$ . In (21),  $c_0$  is a bounded constant. The constant  $c_1$  satisfies  $c_1 > 0$ .  $g_i(t)$  is a time-varying parameter which is selected from the unknown set  $\mathcal{G}_g := [\psi^-, \psi^+]$  (all  $g_i(t)$  have the same sign).

## 4 | ADAPTIVE FAULT-TOLERANT ALTITUDE CONTROL DESIGN

In this section, an adaptive FTC scheme is proposed for the HSV reentry attitude dynamics (1) and (3) subject to unexpected centroid shift, actuator fault and system states constraints. The fault-tolerant control structure is described in Figure 2.

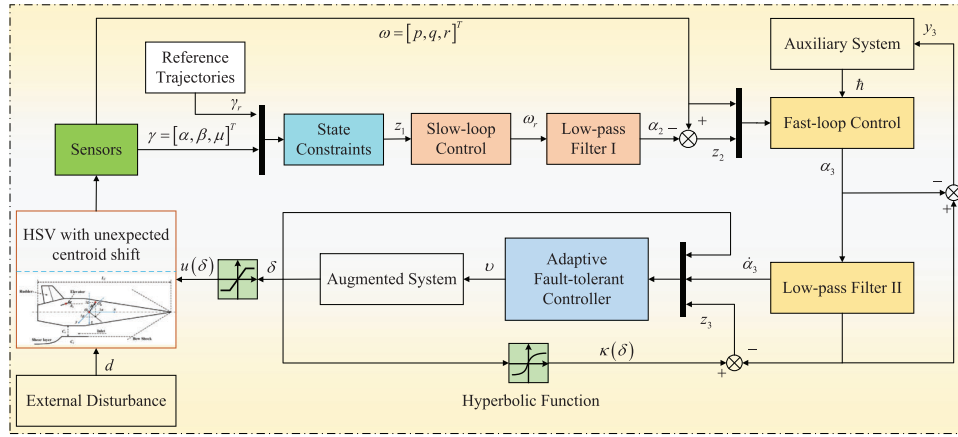


FIGURE 2 Fault-tolerant control block diagram of HSV attitude model with unexpected centroid-shift.

#### 4.1 | Adaptive fault-tolerant controller design

Based on backstepping method, the coordinate transformation is constructed as

$$\zeta_1 = \zeta_1 - \alpha_0, \quad (22a)$$

$$\zeta_2 = \omega - \alpha_{2f}, \quad (22b)$$

$$\alpha_0 = \frac{\gamma_c}{(F_1 + \gamma_r)^T (F_2 - \gamma_r)}, \quad (22c)$$

where  $\zeta_1$  is provided by (15) to handle the time-varying state constraints:

$$\zeta_1 = \frac{\gamma}{(F_1 + \gamma)^T (F_2 - \gamma)}, \quad (23)$$

and  $\zeta_j$  ( $j = 1, 2$ ) denotes the “virtual error,” besides,  $\alpha_{2f} \in R^3$  can be obtained by the first-order filter:

$$\varepsilon_2 \dot{\alpha}_{2f} + \alpha_{2f} = \alpha_1, \quad (24)$$

where  $\varepsilon_2$  is the designed parameter with the positive elements, and  $\alpha_1 \in R^3$  represents the virtual control. Furthermore, we define

$$y_{2,i} = \alpha_{2f,i} - \alpha_{1,i}, \quad i = 1, 2, 3, \quad (25)$$

which facilitates the stability analysis, as seen shortly.

Now, the control design process is carried out step by step.

**Step 1:** By taking derivative of  $\zeta_1$  in (23) with respect to time, it is straightforward to show that

$$\dot{\zeta}_1 = \eta_1 \dot{\gamma} + \eta_2, \quad (26)$$

where

$$\eta_1 = \frac{F_1^T(t) F_2(t) + \gamma^T \gamma}{[(F_1(t) + \gamma)^T (F_2(t) - \gamma)]^2},$$

$$\eta_2 = \frac{[(\dot{F}_1^T F_2 + F_1^T \dot{F}_2) + (\dot{F}_2 - \dot{F}_1) \gamma] \gamma}{[(F_1(t) + \gamma)^T (F_2(t) - \gamma)]^2} \quad (27)$$

Thus, the time derivative of  $\zeta_1 = \zeta_1 - \alpha_0$  along (26) is

$$\dot{\zeta}_1 = \eta_1 (\mathfrak{R} \omega + f_1) + \eta_2 - \eta_{\gamma 1} \dot{\gamma}_c - \eta_{\gamma 2} \quad (28)$$

where

$$\eta_{\gamma 1} = \frac{F_1^T(t) F_2(t) + \gamma_c^T \gamma_c}{[(F_1(t) + \gamma_c)^T (F_2(t) - \gamma_c)]^2},$$

$$\eta_{\gamma 2} = \frac{[(\dot{F}_1^T F_2 + F_1^T \dot{F}_2) + (\dot{F}_2 - \dot{F}_1) \gamma_c] \gamma_c}{[(F_1(t) + \gamma_c)^T (F_2(t) - \gamma_c)]^2}$$

are the computable and bounded functions in the set  $\mathcal{G}$ .

Afterwards, recalling the definition of  $\zeta_2$  and  $y_2$  as given in (22b) and (25) respectively, we have

$$\omega = \zeta_2 + y_2 + \alpha_1, \quad (29)$$

which leads to

$$\dot{\zeta}_1 = \eta_1 \mathfrak{R} \zeta_2 + \eta_1 \mathfrak{R} y_2 + \eta_1 \mathfrak{R} \alpha_1 + \eta_1 f_1 + \eta_2 - \eta_{\gamma 1} \dot{\gamma}_c - \eta_{\gamma 2}. \quad (30)$$

To continue, the derivative of  $\frac{1}{2} \zeta_1^T \zeta_1$  is

$$\zeta_1^T \dot{\zeta}_1 = \zeta_1^T \eta_1 \mathfrak{R} \alpha_1 + \Xi_1, \quad (31)$$

where  $\Xi_1 = \zeta_1^T (\eta_1 \mathfrak{R} \zeta_2 + \eta_1 \mathfrak{R} y_2 + \eta_1 f_1 + \ell_0)$  and  $\ell_0 = \eta_2 - \eta_{\gamma 1} \dot{\gamma}_c - \eta_{\gamma 2}$ . According to Young's inequality, it can be concluded that

$$\zeta_1^T \eta_1 f_1 \leq \underline{\mathfrak{R}} \|\zeta_1\|^2 \eta_1^2 \|f_1\|^2 + \frac{1}{4\underline{\mathfrak{R}}}, \quad (32a)$$

$$\tilde{z}_1^T \eta_1 \mathfrak{R} y_2 \leq \frac{\overline{\mathfrak{R}}}{\underline{\mathfrak{R}}} \|\tilde{z}_1\|^2 \eta_1^2 + \frac{1}{4} \|y_2\|^2, \quad (32b)$$

$$\tilde{z}_1^T \ell_0 \leq \underline{\mathfrak{R}} \|\tilde{z}_1\|^2 \|\ell_0\|^2 + \frac{1}{4\underline{\mathfrak{R}}}, \quad (32c)$$

where  $\underline{\mathfrak{R}}$  and  $\overline{\mathfrak{R}}$  are positive constants.

Therefore, we arrive at

$$\Xi_1 \leq \underline{\mathfrak{R}} b_1 \|\tilde{z}_1\|^2 \Phi_1 + \Delta_1 + \tilde{z}_1^T \eta_1 \mathfrak{R} \tilde{z}_2 + \frac{1}{4} \|y_2\|^2, \quad (33)$$

where  $b_1$  is the virtual unknown constant parameter with

$$b_1 = \max \left\{ 1, \|f_1\|^2, \frac{\overline{\mathfrak{R}}}{\underline{\mathfrak{R}}} \right\}. \quad (34)$$

Besides,  $\Phi_1 = \eta_1^2 + \|\ell_0\|^2 > 0$  represents a known and computable scalar function, and  $\Delta_1 = \frac{1}{2\underline{\mathfrak{R}}}$  stands for an unknown positive constant.

The virtual control  $\alpha_1$  is constructed as follows:

$$\alpha_1 = -\frac{1}{\eta_1} (c_1 \tilde{z}_1 + \tilde{z}_1 \hat{b}_1 \Phi_1), \quad (35)$$

$$\dot{\hat{b}}_1 = \lambda_1 \|\tilde{z}_1\|^2 \Phi_1 + \sigma_1 \hat{b}_1, \quad (36)$$

where  $c_1 > 0$ ,  $\lambda_1 > 0$  and  $\sigma_1 > 0$  are design parameters, and  $\hat{b}_1$  is the estimation value of  $b_1$ .

Define the estimate error of  $b_1$  as  $\tilde{b}_1 = b_1 - \hat{b}_1$ . Ideally, the Lyapunov function candidate is selected as

$$V_1 = \frac{1}{2} \tilde{z}_1^T \tilde{z}_1 + \frac{\mathfrak{R}}{2\lambda_1} \tilde{b}_1^T \tilde{b}_1 + \frac{1}{2} y_2^T y_2, \quad (37)$$

Subsequently,  $\dot{V}_1$  can be calculated as

$$\begin{aligned} \dot{V}_1 &\leq \tilde{z}_1^T \dot{\tilde{z}}_1 + \frac{\mathfrak{R}}{\lambda_1} \tilde{b}_1^T \dot{\tilde{b}}_1 + y_2^T \dot{y}_2 \\ &\leq \tilde{z}_1^T g_1 \eta_1^1 \alpha_1 + \frac{g_1}{\lambda_1} b_1 \|\tilde{z}_1\|^2 \Phi_1 + \Delta_1 + \tilde{z}_1^T \eta_1^1 g_1 \tilde{z}_2 \\ &\quad + \frac{1}{4} \|y_2\|^2 - \frac{\mathfrak{R}}{\lambda_1} \tilde{b}_1^T \dot{\tilde{b}}_1 + y_2^T \dot{y}_2. \end{aligned} \quad (38)$$

After substituting (35) and (36) into (38), it follows

$$\begin{aligned} \dot{V}_1 &\leq -\underline{\mathfrak{R}} c_1 \|\tilde{z}_1\|^2 + \frac{\mathfrak{R} \sigma_1}{\lambda_1} \tilde{b}_1^T \tilde{b}_1 + \Delta_1 + \tilde{z}_1^T \eta_1 \mathfrak{R} \tilde{z}_2 + \frac{1}{4} \|y_2\|^2 + y_2^T \dot{y}_2 \\ &\leq -\underline{\mathfrak{R}} c_1 \|\tilde{z}_1\|^2 - \frac{\mathfrak{R} \sigma_1}{\lambda_1} \|\tilde{b}_1\|^2 + \Gamma_1 + \tilde{z}_1^T \eta_1 \mathfrak{R} \tilde{z}_2 + \frac{1}{4} \|y_2\|^2 + y_2^T \dot{y}_2 \end{aligned} \quad (39)$$

where the facts that  $0 < \underline{\mathfrak{R}} \leq \|\mathfrak{R}\|$  in the set  $D_1$  and  $\frac{\mathfrak{R} \sigma_1}{\lambda_1} \tilde{b}_1^T \tilde{b}_1 \leq \frac{\mathfrak{R} \sigma_1}{2\lambda_1} \|\tilde{b}_1\|^2 - \frac{\mathfrak{R} \sigma_1}{2\lambda_1} \|\tilde{b}_1\|^2$  are used, and  $\Gamma_1 = \Delta_1 + \frac{\mathfrak{R} \sigma_1}{2\lambda_1} \|\tilde{b}_1\|^2$ .

By taking account of the expression of  $y_2$  and the first-order filter described by (24) and (25), we have

$$\dot{y}_2 = \dot{\alpha}_{2f} - \dot{\alpha}_1 = -\frac{y_2}{\varepsilon_2} + \dot{h}_1(\cdot), \quad (40)$$

where

$$-\dot{h}_1 = \dot{\alpha}_1 = \frac{\partial \alpha_1}{\partial \eta_1} \dot{\eta}_1 + \frac{\partial \alpha_1}{\partial \tilde{z}_1} \dot{\tilde{z}}_1 + \frac{\partial \alpha_1}{\partial \hat{b}_1} \dot{\hat{b}}_1 + \frac{\partial \alpha_1}{\partial \Phi_1} \dot{\Phi}_1 \quad (41)$$

is continuous function, then the following inequality can be obtained:

$$\begin{aligned} y_2^T \dot{y}_2 &= -\frac{y_2^T y_2}{\varepsilon_2} + y_2^T \dot{h}_1 \\ &\leq \left( \frac{1}{4} - \frac{1}{\varepsilon_2} \right) y_2^T y_2 + \dot{h}_1^T \dot{h}_1 \end{aligned} \quad (42)$$

Therefore, (39) can be derived as

$$\begin{aligned} \dot{V}_1 &\leq -\underline{\mathfrak{R}} c_1 \|\tilde{z}_1\|^2 - \frac{\mathfrak{R} \sigma_1}{\lambda_1} \|\tilde{b}_1\|^2 + \Gamma_1 + \dot{h}_1^T \dot{h}_1 + \tilde{z}_1^T \eta_1 \mathfrak{R} \tilde{z}_2 \\ &\quad + \left( \frac{1}{2} - \frac{1}{\varepsilon_2} \right) y_2^T y_2. \end{aligned} \quad (43)$$

Choose  $\frac{1}{\varepsilon_2} \geq \frac{1}{2} + \varepsilon_2^*$ , where  $\varepsilon_2^* > 0$  is a positive constant to be designed, then (43) is rewritten as follows:

$$\begin{aligned} \dot{V}_1 &\leq -\underline{\mathfrak{R}} c_1 \|\tilde{z}_1\|^2 - \frac{\mathfrak{R} \sigma_1}{\lambda_1} \|\tilde{b}_1\|^2 + \varepsilon_2^* y_2^T y_2 \\ &\quad + \tilde{z}_1^T \eta_1 \mathfrak{R} \tilde{z}_2 + \Gamma_1 + \dot{h}_1^T \dot{h}_1, \end{aligned} \quad (44)$$

in which the term  $\tilde{z}_1^T \eta_1 \mathfrak{R} \tilde{z}_2$  will be coped with in Step 2 and  $\dot{h}_1$  will be dealt with in Step 3.

**Step 2:** The uncertainty of inertial matrix  $\Delta J$  in (6) follows the potential irreversibility of  $J$  and the time-varying coefficient matrix  $Y$  of (14). Therefore, inspired by [40] and combined with Assumption 2, the following dynamic system is tactfully constructed:

$$\dot{v} = -\kappa_v v + g(v_c), \quad v_c(0) = 0, \quad (45)$$

where  $\kappa_v = \kappa_v^T > 0$ ,  $v_c$  represents an auxiliary intermediate state to be designed,  $g(v_c)$  is a hyperbolic tangent function. For the purpose of handling the input saturation, we design an auxiliary system:

$$\dot{h} = \kappa_h h + (v - g(v_c)), \quad (46)$$

where  $\kappa_h$  is a positive definite diagonal matrix to be designed.

Define  $\tau = \delta$ , and the error can be expressed as

$$\tilde{z}_3 = \tau - \varpi, \quad (47)$$

where  $\varpi$  is constructed based on the following low-pass filter:

$$\epsilon \dot{\varpi} = -\varpi + \nu, \quad \varpi(0) = 0, \quad (48)$$

where  $\epsilon$  is a positive time constant to be chosen. Besides, in (22b) and (22c),  $\alpha_{2f}$  and  $\nu$  are stabilizing functions. For the convenience of analysis, the filter error is defined as  $y_3 = \varpi - \nu$ .

Considering (3), (14), (22) and (48), we obtain

$$J\dot{\tilde{z}}_2 = -\omega^\times J\omega - J\dot{\alpha}_{2f} + BY(\tilde{z}_3 + \varpi) + \eta_\tau + d, \quad (49)$$

where  $\eta_\tau = \Lambda + F\varepsilon(\tau) + \bar{u}$  stands for the complex disturbances caused by unexpected centroid shift, the fault and saturation of control surfaces. In order to simplify analysis, define  $R = -\omega^\times J\omega - J\dot{\alpha}_{2f}$ . It can be observed that  $R$  is linear function with respect to  $J$ . Therefore, a linear operator  $L(\cdot) : R^3 \rightarrow R^{3 \times 6}$  is proposed: for  $\forall x \in R^3$ , one yields  $Jx = L(x)\theta$ , where  $\theta = [J_{11}, J_{12}, J_{13}, J_{22}, J_{23}, J_{33}]^T$  with  $J_{ij}$  being the element of  $J$ . Consequently,  $R$  could be linearly parameterized as  $R = Y(\cdot)\theta$  where  $Y(\cdot) \in R^{3 \times 6}$  is a known regression matrix made as

$$Y(\cdot) = -\omega^\times L(\omega) - L(\dot{\alpha}_{2f}). \quad (50)$$

Similar to [34], define  $b_2 = [\|\theta\|, \bar{\eta}_\tau, d_m]^T$  and  $\Theta_2 = [\|Y(\cdot)\|, 1, 1]^T$ . Then, recalling Assumption 3, the following inequality holds:

$$\|Y(\cdot)\theta + \eta_\tau + d\|^2 \leq \|Y(\cdot)\theta\|^2 + \|\eta_\tau\|^2 + \|d\|^2 \leq b_2^T \Theta_2. \quad (51)$$

According to Lemma 1 in [40], it can be concluded that  $BYB^T$  is a positive definite matrix for  $\forall t \in R$ , so  $\sigma \leq \min(BYB^T)$  holds, where  $\sigma > 0$  is a constant.

Define  $\lambda = 1/\sigma$ ,  $b = \lambda b_\Delta = [\lambda b_2^T, \lambda b_2]^T$ , and  $\Theta = [\Theta_2^T, \|B\|]^T$ , where  $b > 0$  is a constant. For the purpose of designing control law and analysing the stability of the closed-loop system, consider the following Lyapunov function candidate:

$$V_2 = V_1 + \frac{1}{2}\tilde{z}_2^T J \tilde{z}_2 + \frac{\sigma}{2\vartheta_b} \tilde{b}^T \tilde{b} + \frac{\sigma}{2\vartheta_\lambda} \tilde{\lambda}^2, \quad (52)$$

where  $\hat{b}$  and  $\hat{\lambda}$  are the estimations of  $b$  and  $\lambda$ , respectively. Their estimation errors are defined as  $\tilde{b} = b - \hat{b}$  and  $\tilde{\lambda} = \lambda - \hat{\lambda}$ . Besides,  $\vartheta_b$  and  $\vartheta_\lambda$  represent the design parameters. Then, differentiating (52) and recalling (49) yields

$$\begin{aligned} \dot{V}_2 = & \dot{V}_1 + \tilde{z}_2^T BY(\tilde{z}_3 + \varpi) + \tilde{z}_2^T (R + \eta_\tau + d) - \frac{\sigma}{2\vartheta_b} \tilde{b}^T \dot{\tilde{b}} \\ & - \frac{\sigma}{2\vartheta_\lambda} \tilde{\lambda} \dot{\tilde{\lambda}} \end{aligned}$$

$$\begin{aligned} \leq & \dot{V}_1 + \tilde{z}_2^T BY(\tilde{z}_3 + y_3 + \nu) - b_3 \|B\| \|\tilde{z}_2\| + b_\Delta^T \Theta \|\tilde{z}_2\| \\ & - \frac{\sigma}{2\vartheta_b} \tilde{b}^T \dot{\tilde{b}} - \frac{\sigma}{2\vartheta_\lambda} \tilde{\lambda} \dot{\tilde{\lambda}} \end{aligned} \quad (53)$$

Then, add and subtract  $b_3 \|B\| \|\tilde{z}_2\|$  to the right side of the inequality (53) at the same time, and the above inequality (53) can be calculated as

$$\begin{aligned} \dot{V}_2 \leq & \dot{V}_1^* + \tilde{z}_2^T \sigma \lambda \Phi_2 + \tilde{z}_2^T BY\nu + \tilde{z}_2^T BY(\tilde{z}_3 + y_3) \\ & - b_3 \|B\| \|\tilde{z}_2\| + \sigma b^T \Theta \|\tilde{z}_2\| - \frac{\sigma}{2\vartheta_b} \tilde{b}^T \dot{\tilde{b}} - \frac{\sigma}{2\vartheta_\lambda} \tilde{\lambda} \dot{\tilde{\lambda}} \end{aligned} \quad (54)$$

where  $\dot{V}_1^* = \dot{V}_1 - \tilde{z}_2^T \Phi_2$  and  $\Phi_2$  is designed for eliminating the coupled term in  $V_1$  with the details being

$$\Phi_2 = \Re^T \eta_1 \tilde{z}_1. \quad (55)$$

To continue, we introduce a key inequality: for any  $\varepsilon > 0$  and  $x \in R$ , it yields

$$0 \leq |x| - x\sqrt{x^2 + \varepsilon^2} \leq |x| - x^2(|x| + \varepsilon) < \varepsilon. \quad (56)$$

Further, applying the above inequality (56), it is easily derived that

$$\begin{aligned} \tilde{b}^T \Theta \|\tilde{z}_2\| & \leq \frac{(\tilde{b}^T \Theta)^2 \|\tilde{z}_2\|^2}{\sqrt{(\tilde{b}^T \Theta)^2 \|\tilde{z}_2\|^2 + \varphi^2}} + \varphi \\ \hat{\lambda} \|\Phi\| \|\tilde{z}_2\| & \leq \frac{\hat{\lambda}^2 \|\Phi\|^2 \|\tilde{z}_2\|^2}{\sqrt{\hat{\lambda}^2 \|\Phi\|^2 \|\tilde{z}_2\|^2 + \varphi^2}} + \varphi \end{aligned} \quad (57)$$

where  $\varphi$  is a positive constant to be designed later. What is more, combined with Young's inequality, it can be obtained that

$$\|\tilde{z}_2^T BY(\tilde{z}_3 + y_3)\| \leq \frac{1}{\iota} \|\tilde{z}_2\|^2 + \frac{\iota}{2} \|B\|^2 (\|\tilde{z}_3\|^2 + \|y_3\|^2), \quad (58)$$

where  $\iota > 0$  is a constant.

For the purpose of ensuring the closed-loop system to be stable, the following virtual control law is selected as

$$\nu = N(\xi) \bar{\nu}, \quad (59)$$

$$\bar{\nu} = -B^T (k_2 + k(t)) \tilde{z}_2, \quad (60)$$

and the corresponding adaptive laws are designed as

$$\dot{\xi} = -k_\xi \text{diag}(\tilde{z}_2) \bar{\nu}, \quad (61)$$

$$\dot{\tilde{b}} = \vartheta_b \Theta \|\tilde{z}_2\| - \vartheta_b \ell_1 \tilde{b}, \quad (62)$$

$$\dot{\tilde{\lambda}} = \vartheta_\lambda \|\Phi_2\| \|\tilde{z}_2\| - \vartheta_\lambda \ell_2 \tilde{\lambda}, \quad (63)$$

where  $k_2 > 0$ ,  $k_\xi > 0$ ,  $\vartheta_b > 0$ ,  $\vartheta_\lambda > 0$ , and  $\ell_i > 0$  ( $i = 1, 2$ ) are the controller parameters which is needed to be designed.

Especially, in (59),  $k(t)$  is introduced as

$$k(t) = \frac{(\hat{b}^T \Theta)^2}{\sqrt{(\hat{b}^T \Theta)^2 \|\tilde{z}_2\|^2 + \varphi^2}} + \frac{\hat{\lambda}^2 \|\Phi\|^2}{\sqrt{\hat{\lambda}^2 \|\Phi\|^2 \|\tilde{z}_2\|^2 + \varphi^2}} \quad (64)$$

Inserting (59)–(63) together with the inequalities (57) and (58) into (54),  $\dot{V}_2$  can be rewritten as

$$\begin{aligned} \dot{V}_2 \leq & -\mathfrak{R}_{c1} \|\tilde{z}_1\|^2 - \frac{\mathfrak{R}_{\sigma 1}}{2\lambda} \|\tilde{b}_1\|^2 - \varepsilon_2^* y_2^T y_2 + \tilde{h}^T \tilde{h} + \Gamma_1 \\ & - \left( \kappa_2 \sigma - \frac{1}{\iota} \right) \|\tilde{z}_2\|^2 - \frac{\sigma \ell_1}{2} \tilde{b}_2^T \tilde{b}_2 - \frac{\sigma \ell_2}{2} \tilde{\lambda}^2 - b_3 \|B\| \|\tilde{z}_2\| \\ & + \Xi + \frac{\iota}{2} \|B\|^2 (\|\tilde{z}_3\|^2 + \|y_3\|^2) \\ & + \sum_{i=1}^3 \frac{1}{k_{\xi i}} (-g_i N(\xi) + 1) \dot{\xi}_i, \end{aligned} \quad (65)$$

where  $\Xi = \frac{1}{2} \sigma \ell_1 b_2^T b_2 + \frac{1}{2} \sigma \ell_2 \lambda^2 + 2\sigma \varphi$  is a bounded positive scalar.

**Step 3:** Based on (45)–(47),  $\dot{\tilde{z}}_3$  can be calculated as

$$\dot{\tilde{z}}_3 = -\kappa_v v + v_c - \dot{\tilde{w}} + k_h \tilde{h} \quad (66)$$

In order to construct the controller  $v_c$ , we consider the following Lyapunov function:

$$V_3 = V_2 + \frac{1}{2} \tilde{z}_3^T \tilde{z}_3 + \frac{1}{2} y_3^T y_3. \quad (67)$$

Then, recalling (48) and (66), we have

$$\dot{V}_3 \leq \dot{V}_2 + \tilde{z}_3^T (-\kappa v + v_c - \dot{\tilde{w}} + k_h \tilde{h}) - \frac{\|y_3\|^2}{c} + \|y_3\| \|\dot{v}\| \quad (68)$$

Then, the intermediate control function  $v_c$  is designed as follows

$$v_c = -\kappa_3 \tilde{z}_3 + \kappa v + \dot{\tilde{w}} - k_h \tilde{h}, \quad (69)$$

where  $\kappa_3 > 0$  is the designed parameter.

Then, combined with (68) and (69), by the aid of Young's inequality, we have

$$\dot{V}_3 \leq -\dot{V}_2 - \kappa_3 \|\tilde{z}_3\|^2 - \left( \frac{1}{c} - \frac{1}{2a_1} \|\dot{\tilde{w}}\|^2 \right) \|y_3\|^2 + \frac{a_1}{2}, \quad (70)$$

where  $a_1 > 0$  is a positive constant. Combined with (65), we have that

$$\begin{aligned} \dot{V}_3 \leq & -g_{c1} \|\tilde{z}_1\|^2 - \frac{g_{\sigma 1}}{2\gamma_1} \|\tilde{b}_1\|^2 - \left( \kappa_2 \sigma - \frac{1}{\theta} \right) \|\tilde{z}_2\|^2 \\ & - \frac{\sigma \ell_1}{2} \tilde{b}_2^T \tilde{b}_2 - \frac{\sigma \ell_2}{2} \tilde{\lambda}^2 - \varepsilon_2^* y_2^T y_2 + \Xi + \frac{a_1}{2} + \Gamma_1 \\ & - \left( \kappa_3 - \frac{\theta}{2} \|B\|^2 \right) \|\tilde{z}_3\|^2 \end{aligned}$$

$$\begin{aligned} & - \left( \frac{1}{c} - \frac{1}{2a_1} \|\dot{v}\|^2 - \frac{\theta}{2} \|B\|^2 \right) \|y_3\|^2 + \tilde{z}_2^T B Y \tilde{h} - b_2 \|B\| \|\tilde{z}_2\| \\ & + \sum_{i=1}^3 \frac{1}{k_{\xi i}} (-g_i N(\xi) + 1) \dot{\xi}_i. \end{aligned} \quad (71)$$

## 5 | STABILITY ANALYSIS

In this section, the stability analysis of the whole closed-loop system are given by the following theorem.

**Theorem 1.** Consider the attitude system of HSV described by (1)–(3), with unexpected centroid shift (3) and (8), actuator fault and system input saturation (9)–(14) as well as the time-varying state constraints (15). Suppose that the Assumptions 1–5 hold. If the controller designed in (35), (59) and (69) and the adaptive laws (36), (62) are utilized, then the following properties are achieved:

- (i) All the signals in the closed systems are bounded;
- (ii) The system output  $\gamma$  closely tracks the designed index  $\gamma_r$  in that the tracking errors is ultimately uniformly bounded. Furthermore, the constraint  $\|\mathbf{x}(t)\| \leq F_1$  never be violated under the initial condition  $\|\mathbf{x}(t_0)\| \leq F_1$ .

*Proof.* Based on the definition of (59)–(64), it is obtained that  $\dot{v}$  is a continuous function. As a consequence, for  $\forall \varepsilon > 0$ ,  $\mathfrak{F} := \{(\tilde{z}_1, \tilde{z}_2, \tilde{z}_3, \tilde{b}_1, \tilde{b}_2, y_2, y_3, \tilde{\lambda}) : V_3 < 0\}$  is compact. Therefore,  $\|\dot{v}\|$  has a maximum value  $M$  on the set  $\mathfrak{F}$ . It should be noted that the auxiliary state  $\tilde{h}$  is also bounded on  $\mathfrak{F}$ . Afterwards, selecting  $b_2 \geq \sup_{V_3 \leq \rho} \{\|B\| \|\tilde{h}\|\}$ , we have

$$\tilde{z}_2^T B Y \tilde{h} - b_2 \|B\| \|\tilde{z}_2\| \leq 0. \quad (72)$$

Thus, we can obtain that

$$\begin{aligned} \dot{V}_3 \leq & -g_{c1} \|\tilde{z}_1\|^2 - \frac{g_{\sigma 1}}{2\gamma_1} \|\tilde{b}_1\|^2 - \left( \kappa_2 \sigma - \frac{1}{\theta} \right) \|\tilde{z}_2\|^2 \\ & - \frac{\sigma \ell_1}{2} \tilde{b}_2^T \tilde{b}_2 - \frac{\sigma \ell_2}{2} \tilde{\lambda}^2 - \varepsilon_2^* y_2^T y_2 \\ & + \Xi + \frac{a_1}{2} + \Gamma_1 - \left( \kappa_3 - \frac{\theta}{2} \|B\|^2 \right) \|\tilde{z}_3\|^2 \\ & - \left( \frac{1}{c} - \frac{1}{2a_1} \|\dot{v}\|^2 - \frac{\theta}{2} \|B\|^2 \right) \|y_3\|^2 \\ & + \sum_{i=1}^3 \frac{1}{k_{\xi i}} (-g_i N(\xi) + 1) \dot{\xi}_i, \\ \leq & -\Pi V_3 + N + \sum_{i=1}^3 \frac{1}{k_{\xi i}} (-g_i N(\xi) + 1) \dot{\xi}_i, \end{aligned} \quad (73)$$

where

$$\Pi = \min\{2g_{c1}, c_1, 2\left(\kappa_2 \sigma - \frac{1}{\theta}\right) \lambda_{\max}(J), \kappa_3$$

$$-\frac{\vartheta}{2}\|B\|^2, \sigma_1, \ell_1\eta_1, 2\varepsilon_2^*, 2\left(\frac{1}{c} - \frac{1}{2a_1}\|\dot{v}\|^2 - \frac{\vartheta}{2}\|B\|^2\right), \ell_2\eta_2\}$$

$$\mathcal{N} = \Xi + \frac{a_1}{2} + \Gamma < \infty.$$

Then,  $e^{\Pi t}$  is applied to multiply the both sides of (73). By integrating (73) over  $[0, t]$ , one has

$$V(t) \leq \frac{\mathcal{N}}{\Pi} + V(0)e^{-\Pi t} + \sum_{i=1}^3 \frac{1}{k_{\xi i}} \int_0^t |(-g_i N(\xi) + 1)\dot{\xi}_i| d\tau \quad (74)$$

Because  $g_i$  ( $i = 1, 2, 3$ ) locates in the closed interval  $[\psi^-, \psi^+]$ , combined with (74) and Lemma 1,  $V(t)$ ,  $\xi$ ,  $\int_0^t (-g_i N(\xi) + 1)\dot{\xi}_i d\tau$  are bounded on  $[0, t_f]$ . Based on the positive definition of  $V = V_1 + V_2 + V_3$ ,  $V_1$ ,  $V_2$  and  $V_3$ , it can be obtained that  $V_1$ ,  $V_2$  and  $V_3$  are also bounded over  $[0, t_f]$ . Thus,  $\xi_i$  ( $i = 1, 2, 3$ ) is bounded on  $[0, t_f]$ .

For the purpose of analysing the convergence of the whole closed-loop system states before and after the fault, some expositions and deduces are shown as follows.

By taking integration of (73), we have

$$0 \leq V_3(t) \leq \frac{N}{\Pi} + \left(V_3(0) - \frac{N}{\Pi}\right)e^{-\Pi t} \quad (75)$$

When HSV locates in a normal condition, there is no extra requirement for the system state constraint.  $F_1$  is selected large enough to release the performance of aircraft. By taking  $F_1 \rightarrow \infty$ , we have

$$\|\tilde{z}_1(t)\| \leq \sqrt{\frac{N}{\Pi} + \left(V_3(0) - \frac{N}{\Pi}\right)e^{-\Pi t}} \quad (76)$$

where  $\tilde{z}_1$  ultimately converge to a residual set, which is free from the constrains of  $F_1$ .

When the fault occurs, the attitude states of HSV can be regulated to satisfy the initial conditions meeting the demands of new constraint  $F_1$ . Then, the states of HSV can remain in this prescribed safety set by the designed controller. During  $[t_0, t]$ , the integration of the above inequality (73) is calculated as

$$V_3(t) \leq \int -\Pi V_3 dt + \int N dt + V_3(0) \leq Nt + V_3(0). \quad (77)$$

According to (73) and (77), one has

$$\frac{\mathfrak{F}_b^2 \tilde{z}_1^T \tilde{z}_1}{\mathfrak{F}_b^2 - \tilde{z}_1^T \tilde{z}_1} \leq \vartheta t + V(0) \quad (78)$$

When the fault occurs, (78) is reshaped as

$$(\mathfrak{F}_b^2 + \vartheta t + V(0))e_{\gamma}^T e_{\gamma} \leq \mathfrak{F}_b^2 \vartheta t + \mathfrak{F}_b^2 V(0), \quad (79)$$

$$\tilde{z}_1^T \tilde{z}_1 \leq \frac{\mathfrak{F}_b^2 \vartheta t + \mathfrak{F}_b^2 V(0)}{\mathfrak{F}_b^2 + \vartheta t + V(0)}. \quad (80)$$

According to (80), when  $t \rightarrow \infty$ , we have

$$\tilde{z}_1^T \tilde{z}_1 \leq \mathfrak{F}_b^2. \quad (81)$$

As a conclusion, when HSV does not have fault, there is no extra requirement of system state constraints.  $\mathfrak{F}_b \rightarrow \infty$  is introduced and analyzed. When the fault occurs, the system states should be constrained.  $\mathfrak{F}_b$  can be set with the time of fault occurrence based on the actual situation of the aircraft at that time.

## 5.1 | Parameter projection

The parameter projection algorithm is designed to avoid parameters drifting. As a consequence,  $\hat{b}_1$ ,  $\hat{b}_2$ ,  $\hat{\lambda}$  are constrained to reside inside compact sets  $\Omega_{b_1}$ ,  $\Omega_{b_2}$  and  $\Omega_{\lambda}$ , respectively. The compact sets are introduced as [41–44]:

$$\Omega_{b_i} = \left\{ \hat{b}_i : \underline{b}_i \leq \hat{b}_i \leq \bar{b}_i \right\}, i = 1, 2, \quad (82)$$

$$\Omega_{\lambda} = \left\{ \hat{\lambda} : \underline{\lambda} \leq \hat{\lambda} \leq \bar{\lambda} \right\}, \quad (83)$$

where  $\bar{b}_i$ ,  $\underline{b}_i$  ( $i = 1, 2$ ) and  $\bar{\lambda}$ ,  $\underline{\lambda}$  denote the upper bound and lower bound of  $\hat{b}_i$  and  $\hat{\lambda}$ , respectively. Afterwards,  $\hat{b}_1$ ,  $\hat{b}_2$ ,  $\hat{\lambda}$  are modified as

$$\dot{\hat{b}}_1 = \text{Proj}(\dot{\hat{b}}_1, \gamma_1 \|\tilde{z}_1\|^2 \Phi_1 - \sigma_1 \hat{b}_1), \quad (84)$$

$$\dot{\hat{b}}_2 = \text{Proj}(\dot{\hat{b}}_2, \eta_1 \Theta \|\tilde{z}_2\| - \eta_1 \ell_1 \hat{b}_2), \quad (85)$$

$$\dot{\hat{\lambda}} = \text{Proj}(\dot{\hat{\lambda}}, \eta_2 \|\tilde{g}_1^T \eta_1^1 \tilde{z}_1\| \|\tilde{z}_2\| - \eta_2 \ell_2 \hat{\lambda}). \quad (86)$$

Then, let  $a = [\hat{b}_1, \hat{b}_2, \hat{\lambda}]$  and  $b = [\gamma_1 \|\tilde{z}_1\|^2 \Phi_1 - \sigma_1 \hat{b}_1, \eta_1 \Theta \|\tilde{z}_2\| - \eta_1 \ell_1 \hat{b}_2, \eta_2 \|\tilde{g}_1^T \eta_1^1 \tilde{z}_1\| \|\tilde{z}_2\| - \eta_2 \ell_2 \hat{\lambda}]$ . Therefore, the modified adaptive laws can be rewritten as

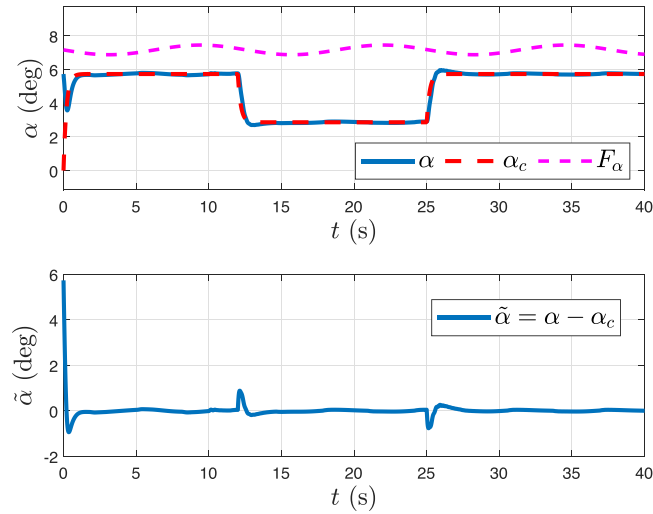
$$\text{Proj}(a_i, b_i) = \begin{cases} 0, & \text{if } a_i = \bar{a}_i, b_i > 0 \\ 0, & \text{if } a_i = \underline{a}_i, b_i < 0 \\ b_i, & \text{else} \end{cases} \quad (87)$$

where  $i$  is the lower annotation of the adaptive laws, such as  $i = \{b_1, b_2, \lambda\}$ .

Subsequently, combined with (73) and (75), it is easily concluded that  $V_3$  is bounded. Then, from the definition of  $V_3$ , it implies the boundedness of  $V_1$  and  $V_2$ . Based on boundedness of  $V_1$  and (76), we can refer that the tracking error  $\lim_{F_1 \rightarrow \infty} \tilde{z}_1 = \xi_1 - \alpha_0$  is ultimately uniformly bounded. Further, we can infer from the boundedness of  $V_3$  that  $\tilde{z}_2$ ,  $\tilde{z}_3$ ,  $\tilde{b}_1$ ,  $\tilde{b}_2$ ,  $\tilde{\lambda}$  and  $y_2, y_3$  are bounded.

**TABLE 1** Position limits of the control surface of X-33.

Effector	Notation	Lower bound (deg)	Upper bound (deg)
Right inboard elevons	$\delta_1$	-25	25
Left inboard elevons	$\delta_2$	-25	25
Right body flaps	$\delta_3$	-30	30
Left body flaps	$\delta_4$	-30	30
Right rudders	$\delta_5$	-15	25
Left rudders	$\delta_6$	-15	25
Right outboard elevons	$\delta_7$	-60	30
Left outboard elevons	$\delta_8$	-30	60

**FIGURE 3** Attack angle response in Case 1.

## 6 | SIMULATION STUDY

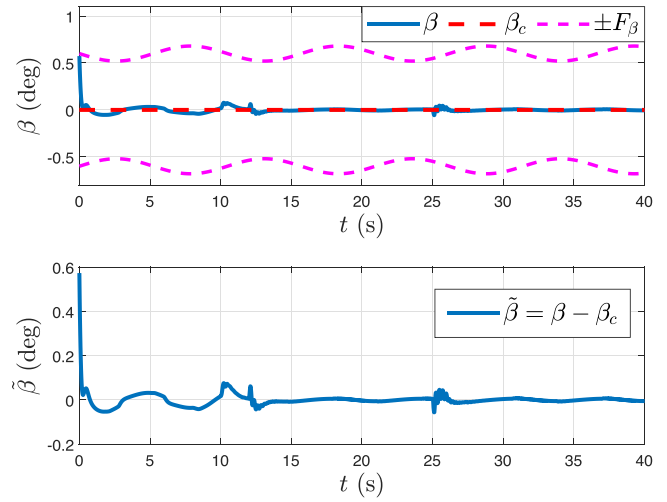
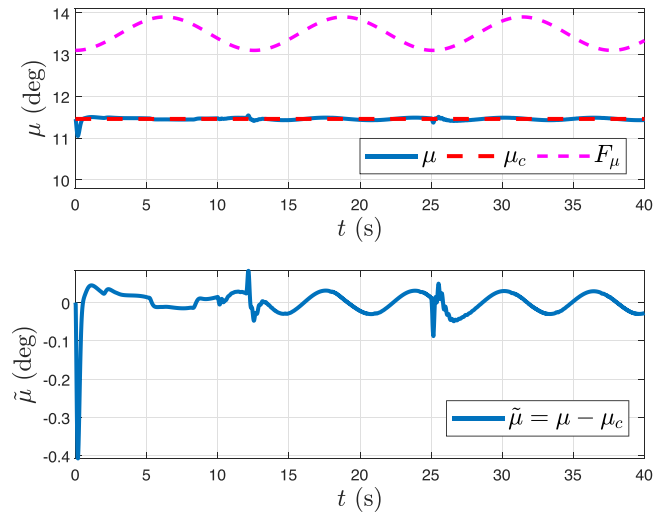
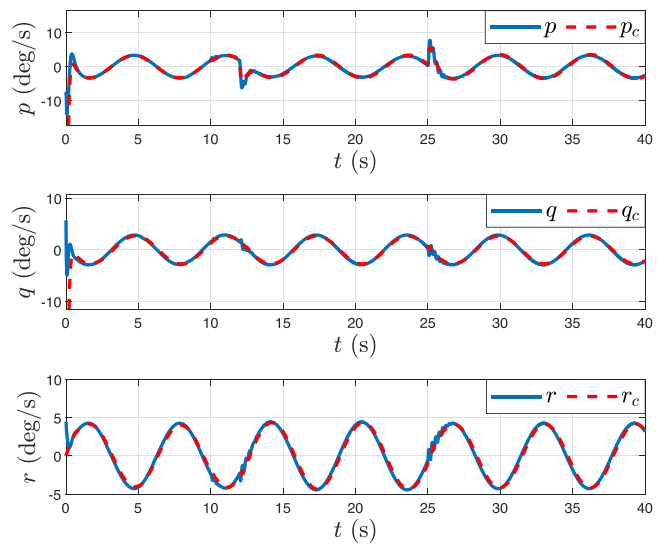
In this section, considering the HSV attitude model suffering from unexpected centroid shift, control surface faults, the simulation results are provided to valid the effective of the proposed FTC scheme.

### 6.1 | Simulation conditions

In simulation, the re-entry vehicle model considered in [45] is discussed. The actuator position limits of the X-33 vehicle are listed in Table 1 [25, 46]. The moment of the inertia matrix is given by [47]

$$J = \begin{bmatrix} 554,486 & 0 & -23,002 \\ 0 & 1,136,949 & 0 \\ -23,002 & 0 & 1,376,852 \end{bmatrix} \quad (88)$$

Consider that the HSV is carrying out a hypersonic reentry flight with the speed of 3 km/s, and the flight altitude is 30 km as well as a mass of  $M = 136,820$  kg. The initial

**FIGURE 4** Sideslip angle response in Case 1.**FIGURE 5** Bank angle response in Case 1.**FIGURE 6** Angular rate responses in Case 1.

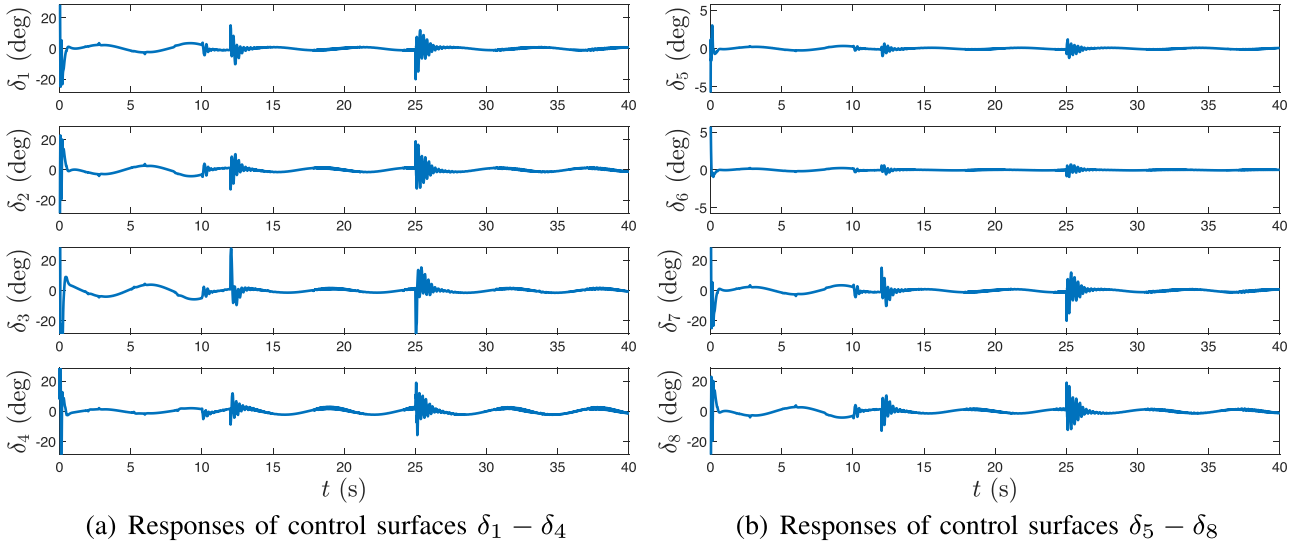


FIGURE 7 Responses of control surfaces in Case 1.

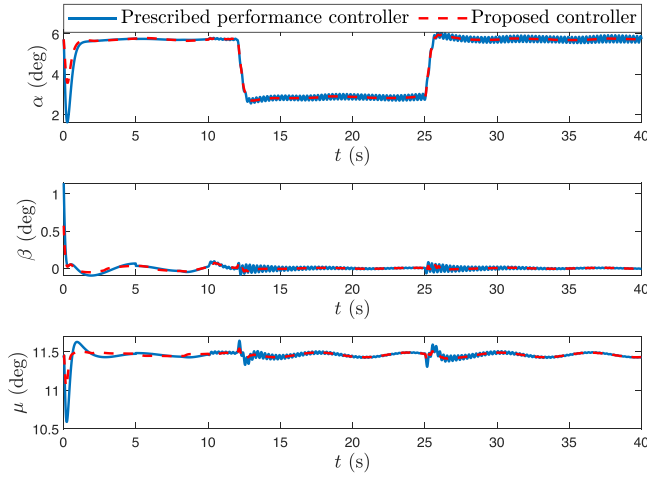


FIGURE 8 Responses of attitude angles with two different methods in Case 1.

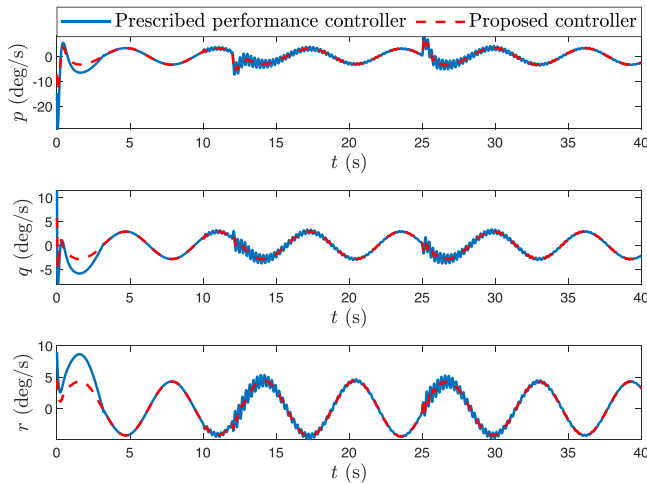


FIGURE 9 Responses of attitude rates with two different methods in Case 1.

values of the system are  $\alpha(0) = 0.1$  rad,  $\beta(0) = 0.01$  rad,  $\mu(0) = 0.2$  rad,  $\dot{p}(0) = 0.1$  rad/s,  $\dot{q}(0) = 0.1$  rad/s,  $\dot{r}(0) = 0.1$  rad/s. The reference trajectories are  $\alpha_c = 0.1$  rad among 1–12 s,  $\alpha_c = 0.25$  rad during 12–25 s and  $\alpha_c = 0.1$  rad during  $t > 25$  s. During the whole simulation,  $\beta$  stays at 0 rad and  $\mu$  maintains at 0.2 rad. The full-state constraints are listed as follows:  $F_\alpha = 7.2 - 0.3 \times \sin(0.5t)$  deg,  $F_\beta = 0.6 - 0.08 \times \sin(0.6t)$  deg and  $F_\mu = 13.5 - 0.4 \times \cos(0.5t)$  deg. The disturbance of HSV fast-loop is set as  $d = [0.05 \sin(t), 0.08 \sin(t), 0.03 \sin(t)]^T$ . As for the fault-tolerant controller, the partial parameters of slow-loop of HSV are that  $c_1 = 4$ ,  $\lambda_1 = 0.2$  and  $\sigma_1 = 0.1$ , and the initial value  $\hat{b}_1$  are set as  $\hat{b}_1(0) = 0$ . As for the fast control-loop of HSV, the design parameters are chosen as  $\hat{b}(0) = 0$ ,  $\hat{\lambda}(0) = 0$ ,  $\varepsilon_2 = 0.01$ ,  $\epsilon = 0.01$ ,  $k_2 = \text{diag}\{0.5, 0.5, 0.5\}$ ,  $k_\xi = \text{diag}\{0.05, 0.03, 0.05\}$ ,  $\vartheta_b = 8$ ,  $\vartheta_\lambda = 10$ ,  $\ell_1 = 0.002$ ,  $\ell_2 = 0.005$ ,  $k_3 = \text{diag}\{3.5, 3.5, 3.4\}$ ,  $\kappa_v = 3$ ,  $\kappa_h = 2.5$ .

## 6.2 | Simulation results and analysis

In order to analyze the bad influence of unknown centroid shift and control surface fault, the simulation is made by two cases. In case 1, we give the simulation results to focus on the HSV model with the unknown centroid shift, failure of actuator as well as disturbance. In Case 2, the comparative simulation is carried out to further verify the effectiveness of the proposed fault-tolerant control.

**Case 1:** In this case, the actuator fault and centroid shift appear in the system. We set the actuator fault with  $F = \text{diag}\{0.2, 1, 0, 0.3, 1, 0.3, 1, 0\}$  and  $\bar{u} = [0, 0, 0.2, 0, 0, 0, 0, 0.2]^T$ . The fault occurrence time is  $t_f = 10$  s. Besides, the centroid shift also occurs in 10 s, matching  $[\Delta x, \Delta y, \Delta z]^T = [25, 24, 23]^T$  cm. The simulation results for this case are shown in Figures 3–9.

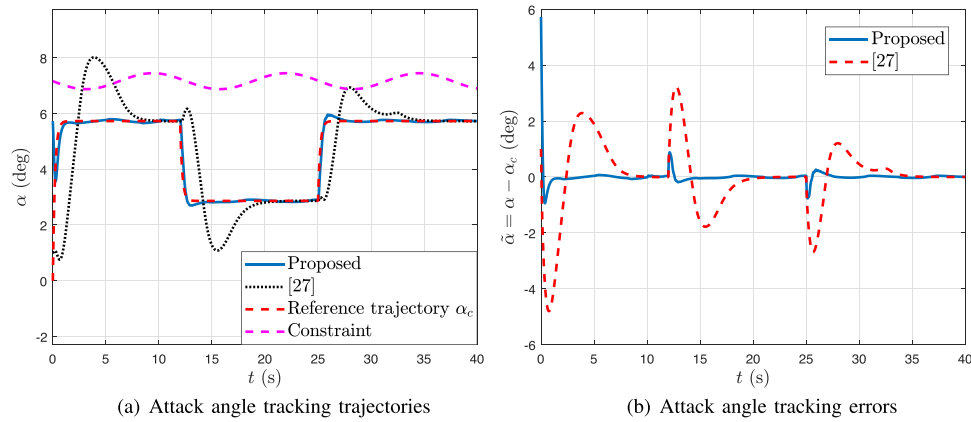


FIGURE 10 Attack angle response in Case 2.

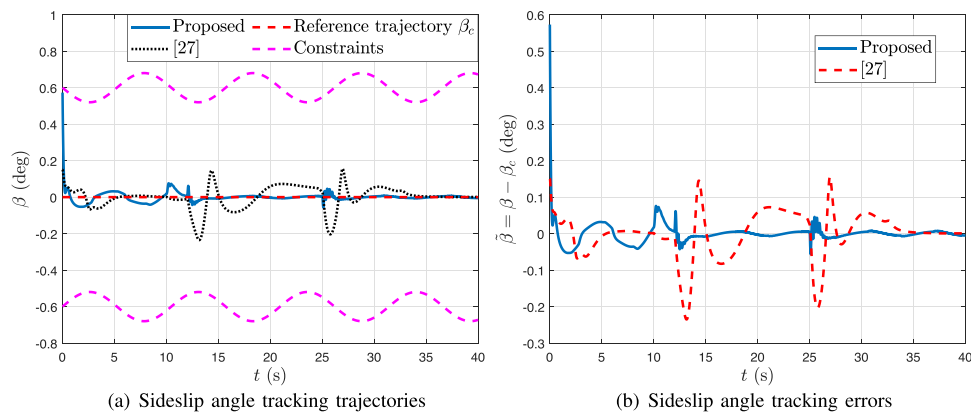


FIGURE 11 Sideslip angle response in Case 2.

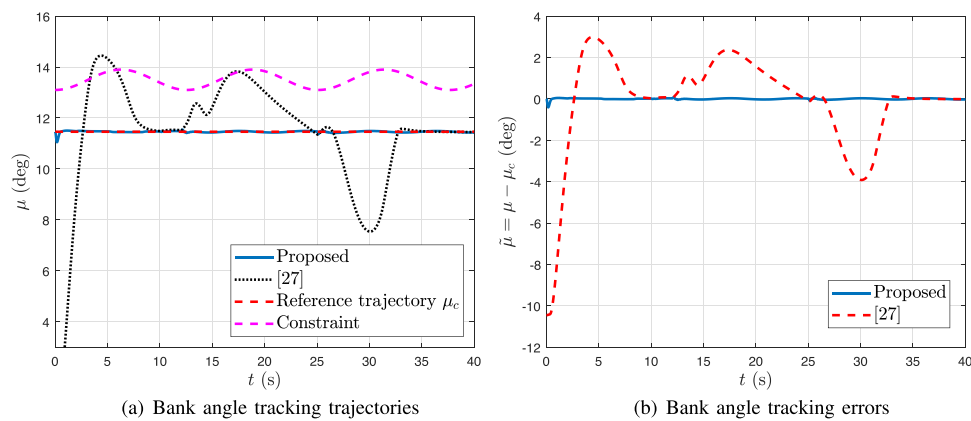


FIGURE 12 Bank angle response in Case 2.

Figures 3–5 depict the output tracking performances of the proposed method. Before the fault and centroid shift occur (before 10 s), the output responses show the good tracking effect. After 10 s, when the actuator fault and centroid shift occur, attack angle  $\alpha$ , sideslip angle  $\beta$  and bank angle  $\mu$  have some transient oscillations. After 10–12 s, the simulation results

are still good. The reason is that the actuator fault, eccentric moments and system can also be estimated. After 12 s, the larger deflection of control surface is needed to satisfy the demand of the preset reference trajectories. In addition, from Figures 3–5, it is obviously observed that all the HSV system outputs are within the predefined time-varying constraints under the

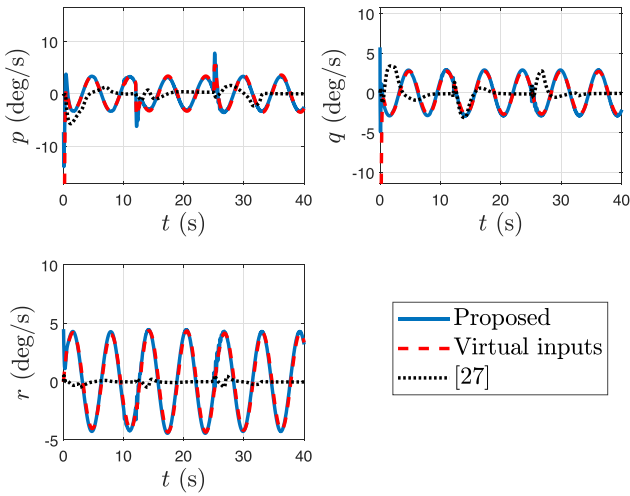


FIGURE 13 Angular rate responses in Case 2.

proposed controller. Figure 6 shows that the system states: roll rate  $p$ , pitch rate  $q$  and yaw rate  $r$  remain stable and tracking the virtual input signals as well. The deflections of control surfaces  $\delta_1 - \delta_8$  are shown in Figure 7, from which it can be seen that the responses of  $\delta_1 - \delta_8$  have some transient oscillations when the actuator fault and centroid shift occur at 10 s, which means the remaining fault-free control surfaces can automatically compensate the actuator faults and maintain the whole control system to be stable.

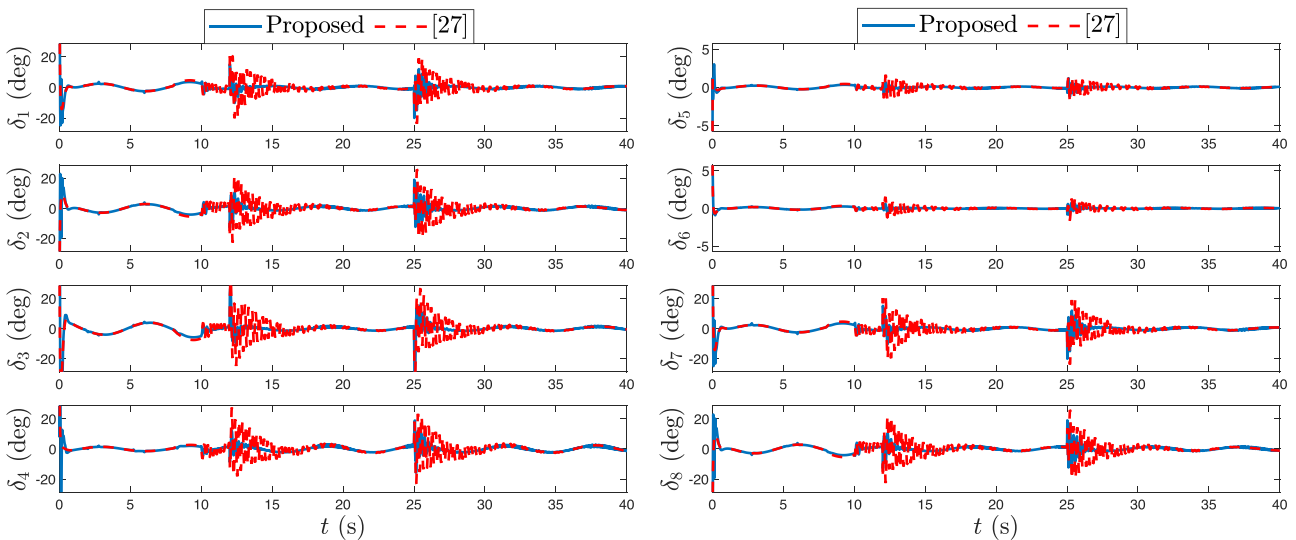
To verify the effectiveness of the proposed FTC strategy under the time-varying full state constraints, we compare the proposed controller with prescribed performance control method in [34]. The paper [34] employs a decaying function of time to predefine a bounded region for restricting the tracking error, but the prescribed performance control scheme is only valid around certain work points. The comparative

simulation results for this case are shown in Figures 8 and 9. It can be seen that our proposed controller owns the more satisfactory tracking performance than that in [34]. In particular, when the reference trajectory  $\alpha_c$  changes at 12 and 25 s, the method in [34] takes more time to ensure the tracking error within the predefined bounded region, which results in the chattering phenomenon.

**Case 2:** In this case, to further verify the effectiveness of the proposed fault-tolerant control strategy, we compare our scheme with the nonlinear general predictive control method given by [27] for HSV.

In [27], the HSV model is divided into a short-period subsystem and a long-period subsystem based on response time. A sliding mode controller is designed for the slow-subsystem of HSV, and a nonlinear general predictive controller is developed for the fast-subsystem, in which the state constraints are not taken into consideration. The simulation conditions are all same with the above mentioned. The comparative simulation results for this case are shown in Figures 10–14.

Figures 10–12 depict the comparative output response curves. It can be observed that the transient responses of the HSV system outputs have been significantly improved using the proposed FTC strategy. Moreover, compared with the responses with or without state constraint, we have that the output responses exceed the preset constraints based on the controller provided in [27]. Figure 13 shows the responses of attitude angular rate ( $p, q, r$ ), from which it can be seen that compared with the simulation curves without state constraints, the angular rates based on the proposed method can better track the corresponding virtual input signals. In Figure 14, the deflections of the control surfaces are shown. It can be observed that the input curves of the control method in [27] have a bad transient performance with large overshoot and long stability time. In summary, when the states of HSV are constrained by the modified barrier Lyapunov function, the simulation results with



(a) Responses of control surfaces  $\delta_1 - \delta_4$

(b) Responses of control surfaces  $\delta_5 - \delta_8$

FIGURE 14 Responses of control surfaces in Case 2.

**TABLE 2** The tracking performance comparison of different schemes for HSV.

Method	Tracking accuracy (deg)			Convergence times (s)			
	Attack angle	Sideslip angle	Bank angle	Attack angle	Sideslip angle	Bank angle	CPU times (s)
The proposed method	$ \tilde{\alpha}  < 0.0076$	$ \tilde{\beta}  < 0.1488$	$ \tilde{\mu}  < 0.0511$	1.56	3.29	1.24	22.57
The method in [34]	$ \tilde{\alpha}  < 0.0249$	$ \tilde{\beta}  < 0.2034$	$ \tilde{\mu}  < 0.1529$	13.54	12.45	6.27	26.42
The method in [27]	$ \tilde{\alpha}  < 0.0485$	$ \tilde{\beta}  < 0.7157$	$ \tilde{\mu}  < 0.1859$	10.88	35.54	36.68	25.28

state constraint show the good tracking performance. Thus, when designing a fault-tolerant controller, the state constraint should be taken into consideration. The state constraint strategy developed in this paper can be a useful way to handle such a problem.

Finally, in order to illustrate the effective tracking performance of the proposed FTC approach in this paper, we compare the tracking performance of the three different control algorithms in terms of convergence time, tracking accuracy and CPU time. Table 2 gives the tracking performance comparison results. In Table 2,  $\tilde{\alpha}$ ,  $\tilde{\beta}$ , and  $\tilde{\mu}$  denote the tracking errors of attack angle, sideslip angle, and bank angle, respectively; The tracking accuracy denotes the convergence domain of the HSV attitude system output, and the convergence time presents the time when the output tracking error first reaches the corresponding convergence domain. Combined with the comparing results in Figures 3–5, 8–12, and Table 2, we can observe that the proposed method in this paper has higher tracking accuracy and shorter convergence time than others. In addition, the CPU time of the proposed method is shortest among them, which indicates that this scheme has low computational complexity. In summary, the developed fault tolerant controller has more efficient robustness and fault tolerant capacity.

## 7 | CONCLUSION

In this paper, the time-varying full state constraints are introduced into the proposed adaptive FTC method for hypersonic reentry vehicle attitude system with unexpected centroid shift, actuator fault, and input saturation. The adaptive fault-tolerant controller is consisted of back-stepping control and auxiliary control system. The system input saturation and the variation of system input structure are governed by the Nussbaum technology. Besides, to handle the system time-varying state constraints, the modified barrier Lyapunov function method has been developed by introducing a time-varying state constraint function to transform the constrained HSV system into a novel free-constrained system. The whole signals of closed loop system are bounded and the system is stable, which have been proved by the Lyapunov theorem of stability. At last, the simulation results have testified the designed effectiveness of fault-tolerant algorithm. In future work, we will consider the problem that the rudders cannot be used due to the high speed, where the HSV attitude system will have non-minimum phase characteristics. Inspired by the jobs in [9, 48, 49], the output tracking problem of the non-minimum phase HSV system will be investigated with the unexpected centroid shift.

## AUTHOR CONTRIBUTIONS

Le Wang: Methodology, software, supervision, validation, visualization, writing—original draft. Yizhen Meng: Formal analysis, investigation, methodology, resources, validation. Shiqi Hu: Funding acquisition, investigation, writing—review and editing. Zhiyu Peng: Project administration. Wen Shi: Project administration.

## ACKNOWLEDGEMENTS

This work was supported by Postgraduate Research & Practice Innovation Program of Jiangsu Province (No. KYCX20\_0207, KYCX20\_0572), Interdisciplinary Innovation Foundation for Graduates, NUAA (No. KXKCXJJ202008) and China Scholarship Council (No. 202206090189, 202206090190).

## CONFLICT OF INTEREST STATEMENT

The authors declare no conflicts of interest.

## DATE AVAILABILITY STATEMENT

The data that support the findings of this study are available from the corresponding author upon reasonable request.

## ORCID

Le Wang  <https://orcid.org/0000-0002-3320-0848>

Shiqi Hu  <https://orcid.org/0000-0002-6528-7896>

## REFERENCES

1. Wang, L., Qi, R., Peng, Z.: Integrated design of adaptive fault-tolerant control for non-minimum phase hypersonic flight vehicle system with input saturation and state constraints. *Proc. Inst. Mech. Eng., Part G: J. Aerosp. Eng.* 236(11), 2281–2301 (2022)
2. Wang, G., An, H., Wang, Y., Xia, H., Ma, G.: Intelligent control of air-breathing hypersonic vehicles subject to path and angle-of-attack constraints. *Acta Astronaut.* 198, 606–616 (2022)
3. He, J., Qi, R., Jiang, B., Qian, J.: Adaptive output feedback fault-tolerant control design for hypersonic flight vehicles. *J. Franklin Inst.* 352(5), 1811–1835 (2015)
4. Ye, H., Meng, Y.: An observer-based adaptive fault-tolerant control for hypersonic vehicle with unexpected centroid shift and input saturation. *ISA Trans.* 130, 51–62 (2022)
5. Hu, Q., Shi, Y., Shao, X.: Adaptive fault-tolerant attitude control for satellite reorientation under input saturation. *Aerosp. Sci. Technol.* 78, 171–182 (2018)
6. Liu, S., Yan, B., Zhang, T., Zhang, X., Yan, J.: Coverage-based cooperative guidance law for intercepting hypersonic vehicles with overload constraint. *Aerosp. Sci. Technol.* 126, 1–15 (2022)
7. Tang, T., Qi, R., Jiang, B.: Adaptive nonlinear generalized predictive control for hypersonic vehicle with unknown parameters and control constraints. *Proc. Inst. Mech. Eng., Part G: J. Aerosp. Eng.* 233(2), 510–532 (2019)

8. Huang, Y., Qi, R., Tao, G.: An adaptive state tracking control scheme for tcs fuzzy models in non-canonical form and with uncertain parameters. *J. Franklin Inst.* 351(7), 3610–3632 (2014)
9. Wang, L., Qi, R., Wen, L., Jiang, B.: Adaptive multiple-model based fault-tolerant control for non-minimum phase hypersonic vehicles with input saturations and error constraints. *IEEE Trans. Aerosp. Electron. Syst.* 59(1), 519–540 (2023)
10. Wang, L., Qi, R., Jiang, B.: Adaptive actuator fault-tolerant control for non-minimum phase air-breathing hypersonic vehicle model. *ISA Trans.* 126, 47–64 (2022)
11. Wang, L., Qi, R., Jiang, B.: Robust adaptive control for non-minimum phase flexible air-breathing hypersonic vehicles. In: *Proceedings of 2019 Chinese Automation Congress*, pp. 3025–3030. IEEE, Piscataway, NJ (2019)
12. Shtessel, Y., Zhu, J., Daniels, D.: Reusable launch vehicle attitude control using time-varying sliding modes. In: *Proceedings of the Thirty-Fourth Southeastern Symposium on System Theory*, pp. 81–85. IEEE, Piscataway, NJ (2002)
13. Hall, C.E., Shtessel, Y.B.: Sliding mode disturbance observer-based control for a reusable launch vehicle. *J. Guid. Control Dyn.* 29(6), 1315–1328 (2006)
14. Da Costa, R., Chu, Q., Mulder, J.: Reentry flight controller design using nonlinear dynamic inversion. *J. Spacecraft Rockets* 40(1), 64–71 (2003)
15. Juliana, S., Chu, Q., Mulder, J., Van Baten, T.: Flight control of atmospheric re-entry vehicle with non-linear dynamic inversion. *AIAA Guid., Navig., Control Conf. Exhibit* 5330, 1–10 (2004)
16. Wu, S.F., Engelen, C., Babuska, R., Chu, Q.P., Mulder, J.: Intelligent flight controller design with fuzzy logic for an atmospheric re-entry vehicle. *38th Aerosp. Sci. Meet. Exhibit* 174, 1–12 (2000)
17. Mathavaraj, S., Halbe, O., Padhi, R.: Robust control of a reusable launch vehicle in reentry phase using model following neuro-adaptive design. *AIAA Guid., Navig., Control Conf. Exhibit* 8312, 1–25 (2010)
18. Li, J., Gao, C., Jing, W., Wei, P.: Dynamic analysis and control of novel moving mass flight vehicle. *Acta Astronaut.* 131, 36–44 (2017)
19. Nguyen, N., Krishnakumar, K., Kaneshige, J., Nespeca, P.: Dynamics and adaptive control for stability recovery of damaged asymmetric aircraft. *AIAA Guid., Navig., Control Conf. Exhibit* 6049, 1–24 (2006)
20. Li, J., Gao, C., Li, C., Jing, W.: A survey on moving mass control technology. *Aerosp. Sci. Technol.* 82, 594–606 (2018)
21. Gasbarri, P., Sabatini, M., Pisculli, A.: Dynamic modelling and stability parametric analysis of a flexible spacecraft with fuel slosh. *Acta Astronaut.* 127, 141–159 (2016)
22. Lee, T.: Robust adaptive attitude tracking on SO(3) with an application to a quadrotor UAV. *IEEE Trans. Control Syst. Technol.* 21(5), 1924–1930 (2012)
23. Yin, S., Ding, S.X., Xie, X., Luo, H.: A review on basic data-driven approaches for industrial process monitoring. *IEEE Trans. Ind. Electron.* 61(11), 6418–6428 (2014)
24. Shtessel, Y., McDuffie, J., Jackson, M., Hall, C., Gallaher, M., Krupp, D., Hendrix, N.D.: Sliding mode control of the X-33 vehicle in launch and reentry modes. *AIAA Guid., Navig., Control Conf. Exhibit* 4414, 1352–1362 (1998)
25. Xu, D., Jiang, B., Shi, P.: Robust NSV fault-tolerant control system design against actuator faults and control surface damage under actuator dynamics. *IEEE Trans. Ind. Electron.* 62(9), 5919–5928 (2015)
26. Meng, Y., Jiang, B., Qi, R.: Adaptive fault-tolerant attitude tracking control of hypersonic vehicle subject to unexpected centroid-shift and state constraints. *Aerosp. Sci. Technol.* 95 105515, 1–13 (2019)
27. Meng, Y., Jiang, B., Qi, R.: Adaptive non-singular fault-tolerant control for hypersonic vehicle with unexpected centroid shift. *IET Control Theory Appl.* 13(12), 1773–1785 (2019)
28. Meng, Y., Jiang, B., Qi, R.: Modeling and control of hypersonic vehicle dynamic under centroid shift. *Adv. Mech. Eng.* 10(9), 1–21 (2018)
29. Meng, Y., Jiang, B., Qi, R., Liu, J.: Fault-tolerant anti-windup control for hypersonic vehicles in reentry based on ISMDO. *J. Franklin Inst.* 355(5), 2067–2090 (2018)
30. Su, R., Zong, Q., Tian, B., You, M.: Comprehensive design of disturbance observer and non-singular terminal sliding mode control for reusable launch vehicles. *IET Control Theory Appl.* 9(12), 1821–1830 (2015)
31. Shin, J.: Adaptive dynamic surface control for a hypersonic aircraft using neural networks. *IEEE Trans. Aerosp. Electron. Syst.* 53(5), 2277–2289 (2017)
32. Zhai, R., Qi, R., Zhang, J.: Compound fault-tolerant attitude control for hypersonic vehicle with reaction control systems in reentry phase. *ISA Trans.* 90, 123–137 (2019)
33. Shao, X., Hu, Q., Shi, Y., Jiang, B.: Fault-tolerant prescribed performance attitude tracking control for spacecraft under input saturation. *IEEE Trans. Control Syst. Technol.* 28(2), 574–582 (2020)
34. Hu, Q., Shao, X., Guo, L.: Adaptive fault-tolerant attitude tracking control of spacecraft with prescribed performance. *IEEE/ASME Trans. Mechatron.* 23(1), 331–341 (2018)
35. Wang, H., Daley, S.: Actuator fault diagnosis: An adaptive observer-based technique. *IEEE Trans. Autom. Control* 41(7), 1073–1078 (1996)
36. Kabore, R., Wang, H.: Design of fault diagnosis filters and fault-tolerant control for a class of nonlinear systems. *IEEE Trans. Autom. Control* 46(11), 1805–1810 (2001)
37. Yin, S., Gao, H., Qiu, J., Kaynak, O.: Adaptive fault-tolerant control for nonlinear system with unknown control directions based on fuzzy approximation. *IEEE Trans. Syst. Man Cybern. Syst.* 47(8), 1909–1918 (2017)
38. Ge, S.S., Wang, J.: Robust adaptive tracking for time-varying uncertain nonlinear systems with unknown control coefficients. *IEEE Trans. Autom. Control* 48(8), 1463–1469 (2003)
39. Jiang, P., Chen, H., Bamforth, L.C.A.: A universal iterative learning stabilizer for a class of MIMO systems. *Automatica* 42(6), 973–981 (2006)
40. Shao, X., Hu, Q., Shi, Y., Jiang, B.: Fault-tolerant prescribed performance attitude tracking control for spacecraft under input saturation. *IEEE Trans. Control Syst. Technol.* 28(2), 574–582 (2020)
41. Hu, Q., Meng, Y., Wang, C., Zhang, Y.: Adaptive backstepping control for air-breathing hypersonic vehicles with input nonlinearities. *Aerosp. Sci. Technol.* 73, 289–299 (2018)
42. Zhao, T., Liu, Y., Li, Z., Su, C.Y., Feng, Y.: Adaptive control and optimization of mobile manipulation subject to input saturation and switching constraints. *IEEE Trans. Autom. Sci. Eng.* 16(4), 1543–1555 (2019)
43. Peng, Z., Qi, R., Jiang, B.: Adaptive fault tolerant control for hypersonic flight vehicle system with state constraints. *J. Franklin Inst.* 357(14), 9351–9377 (2020)
44. Liu, Y., Zhang, H., Wang, Y., Sun, S.: Adaptive fuzzy control for nonstrict-feedback systems under asymmetric time-varying full state constraints without feasibility condition. *IEEE Trans. Fuzzy Syst.* 29(5), 976–985 (2021)
45. Luo, Y., Serrani, A., Yurkovich, S., Oppenheimer, M.W., Doman, D.B.: Model-predictive dynamic control allocation scheme for reentry vehicles. *J. Guid. Control Dyn.* 30(1), 100–113 (2007)
46. Hollis, B.R., Thompson, R.A., Berry, S.A., Horvath, T.J., Murphy, K.J., Nowak, R.J., Alter, S.J.: X-33 computational aeroheating/aerodynamic predictions and comparisons with experimental data. NASA, Washington, DC, Tech. Rep. NASA/TP-2003-212160 (2003)
47. Du, Y., Wu, Q., Jiang, C., Wen, J.: Adaptive functional link network control of near-space vehicles with dynamical uncertainties. *J. Syst. Eng. Electron.* 21(5), 868–876 (2010)
48. Wen, L., Tao, G., Yang, H., Jiang, B.: Adaptive actuator failure compensation for possibly nonminimum-phase systems using control separation based LQ design. *IEEE Trans. Autom. Control* 64(1), 143–158 (2019)
49. Hu, Q., Li, B., Zhang, Y.: Robust attitude control design for spacecraft under assigned velocity and control constraints. *ISA Trans.* 52(4), 480–493 (2013)

**How to cite this article:** Wang, L., Meng, Y., Hu, S., Peng, Z., Shi, W.: Adaptive fault-tolerant attitude tracking control for hypersonic vehicle with unknown inertial matrix and states constraints. *IET Control Theory Appl.* 17, 1397–1412 (2023).  
<https://doi.org/10.1049/cth2.12470>